

## Reply to Reviewer #1:

We thank the reviewer for the time and efforts she/he spent reading our manuscript and providing valuable suggestions and advices. Please find below a discussion of the reviewer's comments (italic). Changes/additions made to the text are underlined and given in quotes.

*- The combination of geometric retrievals and hyperspectral measurements is new and can give additional cloud structure information. In addition its an important information to analyze angle dependent reflectance properties of the DCC relative to the Sun, but the derived parameter of cloud distance from the geometric retrieval is only one single parameter. The observed area by the imaging instrument depends on the field of view, cloud structure and distance and could lead to a 3D cloud structure, but the simple assumption of a homogenous vertical cloud area within the field of view of a single imaging pixel might lead to errors in the analysis of cloud scattering effects.*

The reviewer is right, that we used a simplified assumption in this work. A complete cloud structure retrieval needs much more efforts. In an upcoming publication (Zinner et al.) such a retrieval based on stereographic methods and the signature within the O2-A band will be presented. However, 3D effects due to horizontal photon transport is reduced at the wavelengths which are used for calculation of the phase index. The free photon path length is reduced due to cloud particle absorption in this spectral range. Marshak et al. (2006) and Martins et al. (2011) discussed the usage of 1D radiative transfer simulations for calculation of reflected radiation from cloud sides at different wavelengths. They concluded, that after adaption of the viewing and zenith angle, 1D assumptions are applicable for wavelengths, where cloud water absorption gets relevant and clouds have an optical thickness larger than 40 (Marshak et al., 2006), which is mostly fulfilled for DCCs. However, for the retrieval of the cloud particle radius the cloud structure gets more important due to a much higher contribution of scattering events.

*- A cloud masking procedure is introduced to distinguish between directly reflected areas of the cloud and diffuse shadow regions. The analysis of the manuscript is restricted to directly reflected areas only, which in fact is a sum of direct and diffuse light.*

*- Why does the described method of the distribution of the cloud phase does work only for direct reflected light of the Sun?*

*- What is the influence of the diffuse light?*

As the three comments above relate to each other, we give a joint response on them.

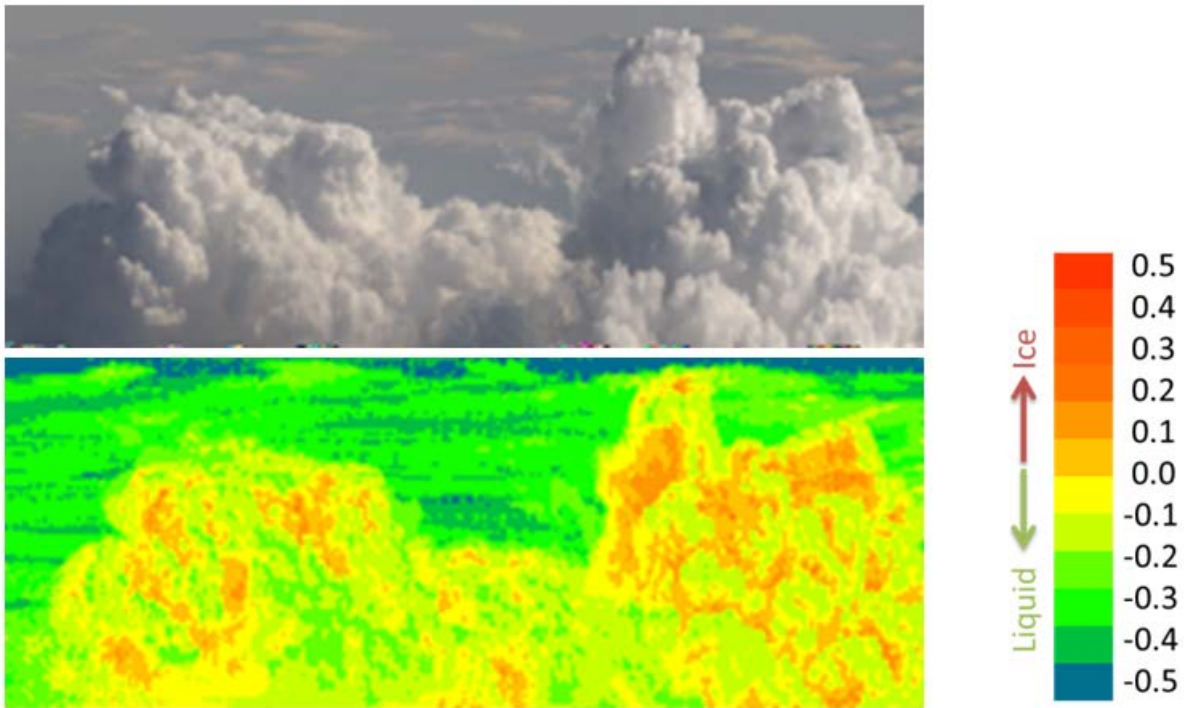
The reviewer makes good point here. In fact it is better to use the phrase "illuminated cloud regions" than talking about directly reflected areas. Of course, the measured reflected radiation contributes both, directly reflected radiation but also diffuse (multiple-scattering) radiation coming from other directions which fall into the sensor viewing angle. Since we are using radiation with wavelengths in the near infrared, the contribution of the diffuse radiation which is in-scattered from other directions is less dominant. For spectral radiation with wavelengths which are affected by Rayleigh scattering this in-scattering would be more relevant.

We added some more explaining sentences in the beginning of the section:

Compared to illuminated cloud sides, the photon paths in shadowed cloud regions are longer, which is related to more absorption events. This absorption due to cloud particles is not locally restricted to the cloud side parts where the camera is pointed at. In fact, the spectral radiation coming from shadowed cloud regions is affected by absorption by cloud particles from cloud parts outside the FOV of each individual spatial camera pixel. Since the spectral signature of

reflected radiation from shadowed regions of cloud sides is contaminated by a significant fraction of diffuse radiation originating from unknown cloud regions, a cloud masking technique was developed to discriminate illuminated and shadowed cloud regions.

For illustration of the effect of shadowed cloud parts we plotted the phase index of a cloud scene without cloud masking below. Flight altitude was about 4 km. All clouds shown here are liquid water clouds, because air temperature is higher than 0°C for this altitude range. The RGB image in the upper panel illustrate the position of the clouds, the lower panel displays the phase index of the same image section. The shadowed cloud regions show a phase index larger than 0.2, which would indicate the presence of ice particles. This illustrates clearly that shadowed cloud regions should be excluded from the data set, because the typical spectral signature of liquid and water clouds is lost.



*- It would be nice to see some more direct and detailed comparisons to the methods of Marshak (2006, reference missing) or Zinner (2008), MODIS, possibly Cloudsat and insitu. The description of Figure 9 could be in much more detail and as the major part from my point of view this is worth more than just one page.*

We surely could use several other satellite observation products for comparing our results, but we limited the measurement strategy to in situ (three instruments already) and the MODIS observations (ensemble method which was already applied for similar studies). The phase retrieval as presented by Marshak et al. (2006) (it's cited now) and Zinner et al. (2008) rely on the same approach. As shown in the reply on comment to Page 3 line 17, there is just a difference of the phase index in absolute numbers, but not in the height of the mixed phase layer itself (see directly reply to Page3 line 17). Furthermore, we modified the application section at various points. The main changes are given below.

When introducing the in situ measurements, we added the following sentences to specify the ideas behind the comparison of the different observation strategies:

The variability of the mixed phase layer in depth and height within a single cloud cluster shows that the vertical distribution at least at the cloud edges is variable. In situ data are used to investigate if such a variability is also observed in the more inner part of the cloud.

Later we added the following:

Furthermore, a second but smaller peak of the particle size was found at about 6 km altitude. From the conceptual model of cloud particle size profiles inside a DCC (e.g., Rosenfeld and Woodley (2003)) it might indicate the bottom of the mixed phase layer, when cloud particle size starts to increase. However, this increase is less pronounced than presented in Rosenfeld and Woodley (2003).

At the end of the subsection we added:

This shows that the satellite-based ensemble method may be representative for a large cloud field. But for individual clouds NIXE-CAPS and specMACS measurements have shown lower glaciation heights. The most likely reason is related to the fact that the ensemble method relies on cloud top observations of growing clouds in different stages of evolution. As shown in Fig. 9g mainly particle sizes between 22 and 27  $\mu\text{m}$  were derived indicating that the profile is dominated by measurements of clouds in the mature stage. At this stage, the particle phase may be altered by up- and downdrafts within the clouds as was shown in Fig. 9e. This leads to an enhanced horizontal variability of the cloud phase state which cannot be resolved by passive remote sensing from cloud top observations. Another, but minor reason of the discrepancy between ensemble method and NIXE-CAPS / specMACS measurements is related to the retrieval uncertainty of the effective cloud particle radius. While scattering properties are well defined for liquid water particles, they are variable for ice particles due to differing habits and crystal shapes (Eichler et al., 2009). This gets even more complicated for cloud tops where phase transition starts. Additional retrieval uncertainties of the particle size directly contribute to the derived profile of  $r_{\text{eff}}$ .

*Page 2 line 5: A mixed phase state of water does not exist. I would rather describe it as an area of phase transition levels from existing state phases eg. from liquid to ice which can vary in temperature gradient, altitude and vertical depth (line 17 is here more precise than 5)*

That is a good point made by the reviewer. We changed the sentence as follows:

DCCs exhibit a high variability of cloud particle sizes and a complex vertical microphysical structure. This includes the different phase states of water (liquid and ice) of the cloud particles and the occurrence of layers where phase transitions between liquid water and ice particles (further referred to as mixed phase) take place.

*Page 2 line 13: ... (more aerosol particles ...)*

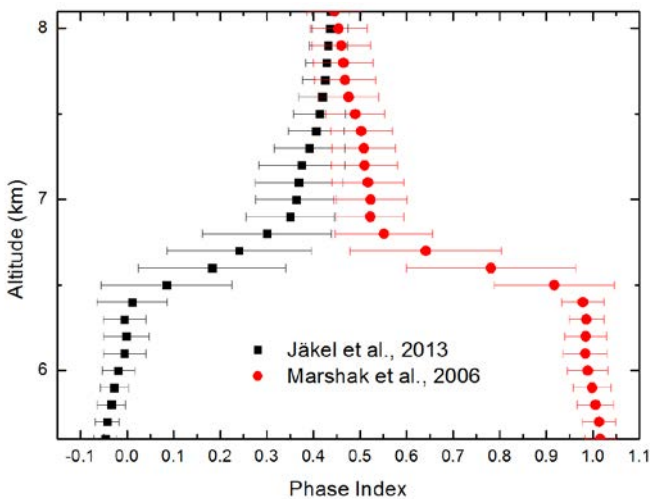
Changed into:

more aerosol particles

*Page 3 line 17: Why did Martins and Marshak use a different Wavelength? With SpecMACS it could be used as well and compared.*

The choice of wavelength pair is originated from the method described by Jäkel et al., (2013) which was designed for spectrometers not measuring at 2.1 and 2.25  $\mu\text{m}$  wavelength. There are

several methods and wavelength ranges used and discussed in the past as listed in the introduction. The change of the sign of the phase index as calculated in this manuscript between liquid and ice phase is kind of illustrative. However, we compared the phase index profile for one of the cases derived by both methods as can be shown in the plot below. Apart from the absolute numbers we see a similar effect within the transition zone with a distinctive slope of both phase indices. So we don't see additional information when using 2.1/2.25  $\mu\text{m}$  instead of radiances between 1550 and 1700 nm. The physics behind for both methods is similar; where the imaginary part of the refractive index which determines the spectral absorption is different between ice and liquid water particles in these two wavelength ranges. So it is not surprising, that the vertical profiles show the indication of the phase transition zone in the same vertical levels.



*Page 4 line 14: Temperature profiles are mentioned and it would be very helpful to have some graphs. Sideways looking IR-camera would be interesting.*

We tried to reduce the number of figures. Therefore, we omitted an individual plot showing the temperature profiles which are similar, as also stated in the overview paper by Wendisch et al., (2016). However, the relations between altitude and temperature can be estimated from the secondary y-axis showing the temperature as vertical coordinate in Fig. 9a for AC13 and in Fig. 10a,b for AC10 and AC18.

The reviewer makes a good point here to bring up the usage of an IR camera. Unfortunately, we had no IR-camera available for this campaign. But another ground-based campaign is scheduled for September/October in 2017 in the Brazilian rainforest using IR-camera and imaging spectrometers together for cloud side observations.

*Page 5 line 2: Again a comparison to the method of Marshak, ... is possible with SpecMACS.*

Please see answer on comment concerning Page 3 line 17.

*Page 5 line 29: mixed phase layer... → phase transition layer*

The “term mixed” phase is commonly used in literature. We are aware that there is no mixed phase state as already commented by the reviewer. But we think the term “mixed phase” is not misleading here. For simplicity and consistency with literature we defined the layers of phase transition between liquid and ice particles as mixed phase in the introduction.

*Page 5 line 29: A retrieval of cloud particle size of the measurements would demonstrate this sentence*

The retrieval of the cloud particle size from cloud side observations needs a lot of efforts and will be presented in a different publication entitled: “How accurately can we remotely sense cloud vertical profiles of droplet radius and phase from the cloud side perspective?” which is in preparation by Ewald et al.

We added a citation here where profiles of particle sizes together with estimations of the phase are presented:

The mixed phase layer is characterized by a strong increase of cloud particle size with height (Martins et al., 2011), whereas for fully glaciated cloud layers the largest ice particles can be found directly at the height where the glaciation temperature is reached.

*Page 6 line 11: Please explain this statement, if its true. Please compare state of polarization with Mie-Theory.*

The scattered and incident intensities of the polarization components are related by the phase function. This phase function is simplified for spherical particles due to their particle symmetry. We will not show the matrix operations here but we added a reference here which describes also mathematically the polarization of aspherical and spherical particles as measured with NIXE-CAPS:

Spherical particles do not strongly alter the polarization state of the incident light as discussed in detail by (Meyer, 2012), while non-spherical ice crystals change the polarization depending on their size and orientation (Nicolet et al., 2007; Meyer, 2012).

*Page 6 line 23 and 30: detection limit unclear. >1 cm<sup>-3</sup> or 0.3 g/m<sup>-3</sup>*

These data and detection limits are from two different instruments integrated in the CAS-DPOL. We use the laser spectrometer on the CAS-DPOL (Cloud and Aerosol Spectrometer) to derive the aspherical particle fraction. Here, the cloud data are given for the size range between 3 and 50  $\mu\text{m}$  and for clouds with a cloud particle number density  $> 1 \text{ cm}^{-3}$ . In addition, the hotwire instrument on the CAS-DPOL measures the liquid water content with a (conservative) detection limit of  $0.3 \text{ g/cm}^{-3}$ .

*Page 7 line 3: Please explain the adjustment of the temperature, humidity, ... profiles*

In particular, the density of water vapor was re-calculated from measured temperature, pressure and relative humidity for each model height level. For simplifications we will not give the equations as they can be read in textbooks.

However, we adapted the sentences as follows:

For the model input, the atmospheric profiles of temperature, atmospheric pressure, and gas densities are taken from Anderson et al., (1986). From a radio sounding from Alta Floresta (-9.866° S, -56.105° W) and measurements of temperature, humidity and pressure performed by HALO, the temperature and pressure profiles are adjusted to represent the atmospheric conditions on 19 September 2014 (AC13) in the region of one of the measurement flights

(representative of the three flights considered in this study). The density of water vapor is recalculated using the relative humidity, temperature and pressure measurements.

*Page 7 line 11: adjustment of the aerosol profile?*

The standard Shettle profile was scaled by the vertically integrated AERONET measurements. We are aware that this adjusted profile is just a rough estimate of the true vertical profile, but it will serve as input for radiative transfer simulations for sensitivity tests concerning cloud microphysical properties. As AOD decreases with wavelength, the aerosol extinction in the wavelength range between 1550 and 1700 nm is less important than cloud particle extinction in this spectral range.

We replaced “adjusted” by “scaled”:

For the polluted case, aerosol properties are described with the model by Shettle (1989) and scaled by AERONET (AErosol ROBotic NETwork) measurements (site Alta Floresta) of aerosol optical depth, single scattering albedo, and asymmetry parameter (used for the Henyey-Greenstein phase function).

*Page 7 line 19: As mentioned before. Why is the diffuse light restricted to shadow regions or does it have the same amount in the other regions as well?*

Please look for response on comments 2-4 above, since it deals with the same topic.

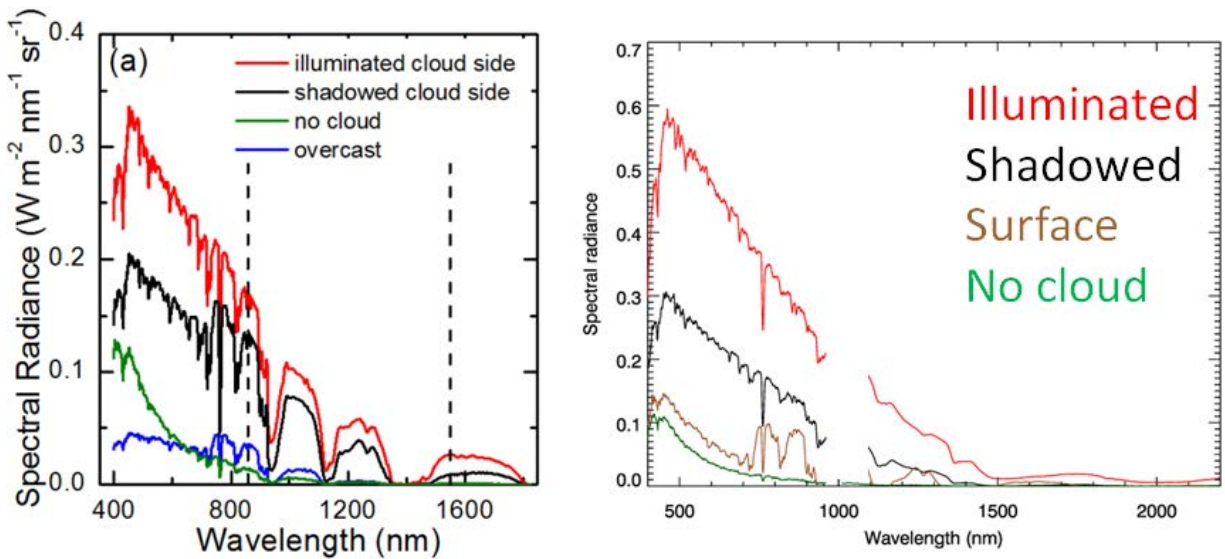
*Page 7 line 21: Here we have some weak indications why the diffuse light in shadow regions is not used in this study. While a thoroughly radiative transfer simulation can include the influence of ground reflectance, surface albedo in this manuscript can't be taken into account because of this influence. Why is that and a view sentences later the influence of the surface can't be seen in the airborne data? The reasoning in this part of the manuscript is somehow very weak.*

The reason for excluding the shadowed cloud regions from data evaluation is given above (see comments 2-4). It is a good question, why the effect of surface reflection was not observed during the aircraft measurements. Compared to ground-based observations, where the spectral features of the surface albedo (here vegetation step around 700 nm) can be found in the spectra of the reflected radiation of shadowed cloud regions (see left panel of the figure below from Jäkel et al., 2013), the cloud and observation geometry is different for the aircraft measurements during ACRIDICON-CHUVA. This is related to changes of the range of scattering angles, because reflected radiation is observed from higher altitudes than from the ground. Furthermore, for deep convective clouds the distance between surface and upper parts of the clouds is enhanced, which reduces the contribution of radiation coming from the surface. However, a detailed model study would be needed to quantify the surface effects on the reflected radiation coming from shadowed cloud regions to estimate the measurement conditions when significant spectral features can be used for shadow detection. Since we didn't observe such features, such a study will not be included in this work. In the figure below, the right panel shows clearly no indication of the vegetation step in the shadowed cloud region, while the surface observation shows the typical increase of radiation above 700 nm wavelength.

We modified this part as follows:

In ground-based observations the reflected radiation measured from shadowed cloud regions showed spectral signatures influenced by the spectral surface albedo due to interaction between clouds and the surface (Jäkel et al., 2013). This interaction is reduced for several reasons for aircraft observation of DCC. The reflected radiation is observed from higher altitudes than from the ground. This is related to changes of the range of scattering angles. Furthermore, the

distances between surface and in particular the upper parts of the cloud are much larger. Therefore, scattered radiation from the immediately adjacent cloud regions has a greater effect on the spectral features in the shadowed cloud areas than the surface. Since spectral indication of the surface could neither be observed nor simulated for airborne measurements, a different approach is chosen based on the distribution of color values in the observed cloud scene.



Page 8 line 29: *Where does this formula and the constants come from? I would propose to use a spectrum to rgb conversion via a CIE 1931 color space. SpecMACS has a broad spectral range and a large number of spectral channels why not using them? This would reduce noise as well.*

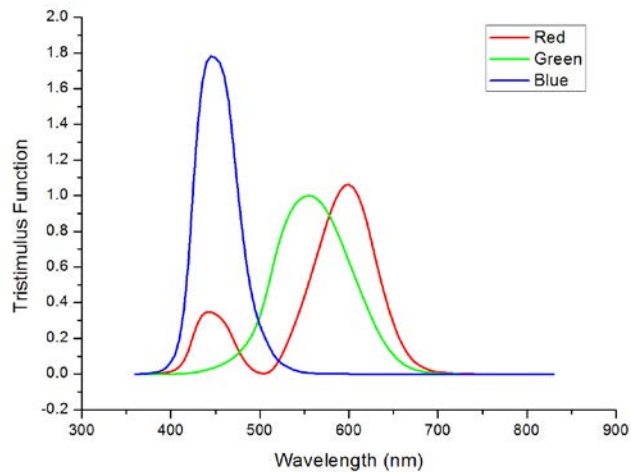
The equation calculates the relative luminance (CIE, 1999). We added the reference:

... which takes into account the sensitivity of the human eye on the different colors by differential weighting of the three wavelengths (IEC, 1999)

IEC: Multimedia Systems and Equipment – Colour Measurements and Management – Part 2-1: Colour Management – Default RGB Color Space – sRGB, IEC 61966-2-1, International Electrotechnical Commission: Geneva, Switzerland, 1999.

We omitted the usage of “relative luminance” in the manuscript because it is a photometric quantity used in digital image processing and less known in the field of atmospheric science. As explained by Magisa et al. (2005), the “relative luminance (RL) is the relative brightness of any point in a color-space, normalized to 0 for the darkest black and 1 for the brightest white. For a certain point (or pixel) in a color image encoded in the standard RGB (sRGB) color-space, the RL can be computed based on the value of the sRGB components through the equation  $RL = 0.2126R + 0.7152G + 0.0722B$ ”.

RGB conversion via CIA 1931 uses a spectral weighting of the red, green, and blue channels, where the weighting function corresponds to the spectral response of the human eye. The color matching function as taken from CIE is shown below:

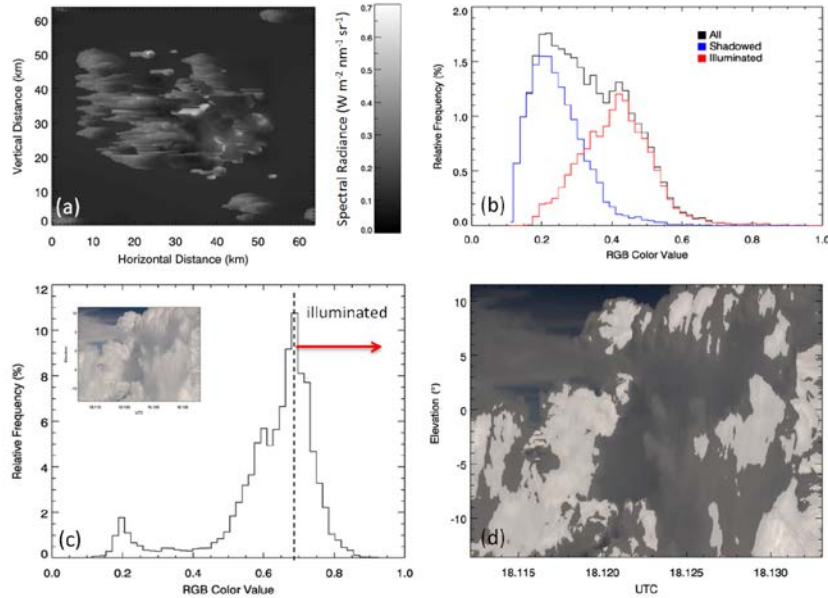


The spectral bandwidth of the three weighting functions is quite broad. If there is a difference in the spectral signature of the radiances between shadowed and illuminated cloud areas, then the usage of CIE bands is not recommended, due to the loss of spectral information after applying the spectral convolution. However, using RGB values to classify the brightness of the individual pixels doesn't require the full spectral information as it could be provided by specMACS. The simple approach to identify the directly illuminated cloud areas based on the three wavelengths (436, 555, 700 nm), has been approved by the simulations.

But for the upcoming ground-based campaign in September/October 2017 we will use the whole spectral information from 400 – 2500 nm to gather information on the illumination conditions as found in Jäkel et al. (2013).

*Page 8 line 1, ...: How is the histogram of the RGB values converted or evaluated to the frequency distribution? Please explain in more detail. Where does the relative and absolute frequency come from in fig. 3? Why are the simulated once in Fig 3b absolute and the measured once in Fig 3c relative? The calculation of a single RGB value with the formula is used to find the threshold of "directly !" illuminated pixels. What are the model simulations for if you dont use them?*

The RGB histogram (= frequency distribution) derived from the simulations was shown to illustrate that such histograms can be used to discriminate between the illuminated and shadowed cloud regions. The threshold estimated from the distribution of the RGB values is just an example and not valid for other cloud scenes with different observation geometry. But we see clearly that the modes in the histogram match with the illuminated and shadowed cloud regions as classified from the known geometry in the model. We plotted now both histograms (from simulation and from measurements) as relative frequency as suggested by the reviewer:



Furthermore, we modified the text:

The histogram of the RGB color values for each cloud scene is used to identify the illuminated and shadowed cloud areas. Before showing an application, the procedure is illustrated using simulated cloud side reflectivity observations. In this manner, we can directly compare the classification of illuminated and shadowed cloud regions (i) derived from known cloud and viewing geometry, and (ii) derived from the histogram of the RGB color values.

And later:

The histogram of the simulated RGB color values is shown in Fig. 3b as black line. Two modes are visible, which coincide with the two sub-classes of illuminated (red) and shadowed (blue) cloud regions as calculated from the cloud and viewing geometry.

*Page 8 line 3: What is the max height of the model domain?*

The maximum height was 120 km corresponding to the top of atmosphere. We added the top height and vertical resolution to the text:

The cloud field was generated by the Goddard Cumulus Ensemble model (Tao et al., 2003, Zinner et al., 2008) for a model domain of 64 x 64 km with a horizontal resolution of 250 m and a vertical resolution between 0 and 10 km altitude of 200 m. From 10 to 120 km altitude the simulations are performed with a vertical resolution ranging between 1 and 5 km. The maximum extension of the liquid water clouds from bottom to cloud top ranges from 1.0 to 7.4 km altitude.

*Page 8 line 16: What is a relative azimuth angle of exactly 68 degree with a changing attitude and Sun elevation during airborne missions?*

The data given here are valid for the cloud scene (about one minute of flight with constant heading) which is shown in the Figure 3. Of course the distribution of RGB color values has to be calculated for each cloud scene separately. It is not meant here, that this histogram and the related threshold is valid for the entire flight. In fact, the thresholds depend on the illumination conditions and viewing geometry. We modified the section to make it clearer for the reader.

The procedure is applied exemplarily for a cloud scene observed during ACRIDICON-CHUVA from 19 September 2014. During the roughly one minute flight leg the aircraft did not change its flight attitude, resulting in almost constant relative azimuth angle (angle between the sun and the viewing direction of specMACS) of 68° and solar zenith angle ( $\theta = 39^\circ$ ). Note, that all other selected cloud cases in this study have similar restrictions concerning the flight attitude and time period (about one minute) to guarantee comparable illumination conditions in one cloud scene. Fig. 3c illustrates the RGB histogram as calculated for observations of specMACS with an elevation ranging between -13 and +12°.

*Page 8 line 22,23: The simulation shows an increase in cloud particle size in Fig 4 for that region. What is wrong?*

In the beginning of Section 3.2 a short motivation is given why a phase index may be a better indicator for the location of the transition layer than using the vertical profile of the cloud effective radius as used by Rosenfeld and Woodley (2003). But as mentioned, there are cases where the particle radius doesn't increase with decreasing temperature. For this reason, we used the phase index.

Fig. 4b shows one example of a profile with variable effective radius and water content. There was no intention to derive the profile of the phase index typical for marine, continental and polluted conditions. We restricted the simulations to two special cases, first, a constant distribution of  $R_{\text{eff}}$  and LWC/IWC with height, where the effect of variations in the microphysical properties (apart from the particle phase) on the phase index can be neglected and second, a typical cloud profile with variable microphysics.

Furthermore, modified the motivation for showing additional radiative transfer simulations:

In the following, results from radiative transfer simulations using MCARATS are presented. The viewing geometry and the atmospheric description are adapted to the conditions during ACRIDICON-CHUVA on 19 September 2014. These simulations are performed to demonstrate that ice and liquid water phase can be separated from the transition layer under different conditions similar to the results reported by Jäkel et al. (2013). Note, that due to the different viewing geometry, another angular range of the scattering phase function is observed than for ground-based measurements. This might have an effect on the characteristics of phase index profile in particular with respect to separation of the mixed phase layer.

And later the two cloud scenarios are introduced as follows:

Two simplified cloud scenarios with different profiles of cloud effective radius and water content are assumed. In both cases the clouds ranged from 4.0 to 11.0 km altitude with a mixed phase layer between 6.4 and 7.0 km. While the first scenario uses constant values of cloud effective radius ( $r_{\text{eff}} = 20 \mu\text{m}$  for liquid water and ice) and water content ( $0.7 \text{ g m}^{-3}$ ), the second scenario assumes variable profiles of the microphysical parameters. These two cases are chosen to identify effects on the  $I_p$ -profile caused by changes of (i) the phase state itself (scenario 1), and changes of (ii) the cloud particle size and water content (scenario 2).

*Page 8 line 28: How does this simple formula compare to the methods from Marshak, Martins and Zinner?*

We gave some additional information:

For ground-based application with corresponding viewing geometry vertical profiles of the phase index were simulated by Jäkel et al. (2013). A significant gradient in the vertical profile of the phase index was observed between liquid water and mixed phase layer, but also between mixed phase layer and ice phase. A similar behavior was also found for the reflectance ratio at 2.10 and 2.25  $\mu\text{m}$  as reported by Martins et al. (2011). They observed a strong gradient in the profile of the reflectance ratio. This is due to the fact, that the imaginary part of the refractive index, which determines the spectral absorption, is different between ice and liquid water particles in the two wavelength ranges used by Martins et al. (2011) and Jäkel et al. (2013).

*Page 9 line 5: Is the combined  $I_p$  profile a simulated or measured profile. I don't understand how the combined profile is calculated and where it comes from.*

We modified the sentences as follows:

From the 3D simulations of the spectral radiance at 1550 and 1700 nm the phase index is calculated following Eq. (2). For each modeled grid cell in the model domain with a horizontal distance between 3 and 8 km to the cloud, a combined  $I_p$ -profile is derived from the different viewing elevation angles. Such  $I_p$ -profiles are plotted in Fig. 4a in black dots.

*Page 9 line 7: three phases ?*

We changed the sentence, also later in line 11.

For the first scenario with constant microphysical parameters, three distinct clusters corresponding to the phase state of water and the zone of phase transition, with negative values for pure liquid water, can be found.

And:

The variability of the phase index for constant microphysical conditions in each of the phases is caused by the effect of the different viewing geometries.

*Page 9 line 10: What is a pronounced absorption, of what?*

Changed as follows:

This might be caused by the fact that the contribution of ice particles within the mixed phase layer leads to an increased absorption of radiation resulting in an increase of the phase index.

*Page 9 line 12: Each cloud height  $\rightarrow$  The cloud vertical structure is ...*

*Changed as suggested:*

The vertical cloud structure is observed from different sensor elevation angles and distances.

*Page 9 line 14: To derive the particle size is first mentioned here. Is that the goal or what is the reason? A look up table would do as well, please look at AMT Zinner 2016.*

It seems that this sentence is misleading. Therefore, we deleted it from the manuscript. The retrieval of the effective radius is not object of this work.

*Page 9 line 15: What is a more realistic cloud? Are the other clouds not realistic?*

We modified this part as follows:

The second cloud scenario assumes variable cloud microphysical properties. In general, in convective clouds, the size of ice particles is higher than the size of liquid water particles. Therefore, the second scenario represents a more realistic vertical distribution of the particle effective radius and water content than the first scenario.

*Page 9 line 17: What is the first case?*

We better introduced now the two cloud setups as used for the radiative transfer simulations and omitted the phrase “case” in this section. See also reply on comment Page 8 line 22,23.

*Page 9 line 18: The transition layer is characterized by a strong increase in particle size and change in the value of phase index. See Fig 4b (simulations) and Fig. 8*

The sentence refers to the description of the microphysical parameters as illustrated in Fig. 4b. Therefore, no information about the phase index is given here. It follows some lines below.

*Page 9 line 24: I assume that we have a polluted and a clear case, but it's not clear in this part of the manuscript. Here we have only two cloud cases, one with fixed microphysics and one with changing cloud properties. Please clarify.*

The two scenarios shown here are intended to demonstrate if the phase index can resolve the three layers with viewing geometry from the aircraft observations. So, we haven't chosen the two scenarios with respect to aerosol conditions. It should be getting clearer for the reader after modification of the beginning of the section (see reply on comment Page 8 line 22,23:)

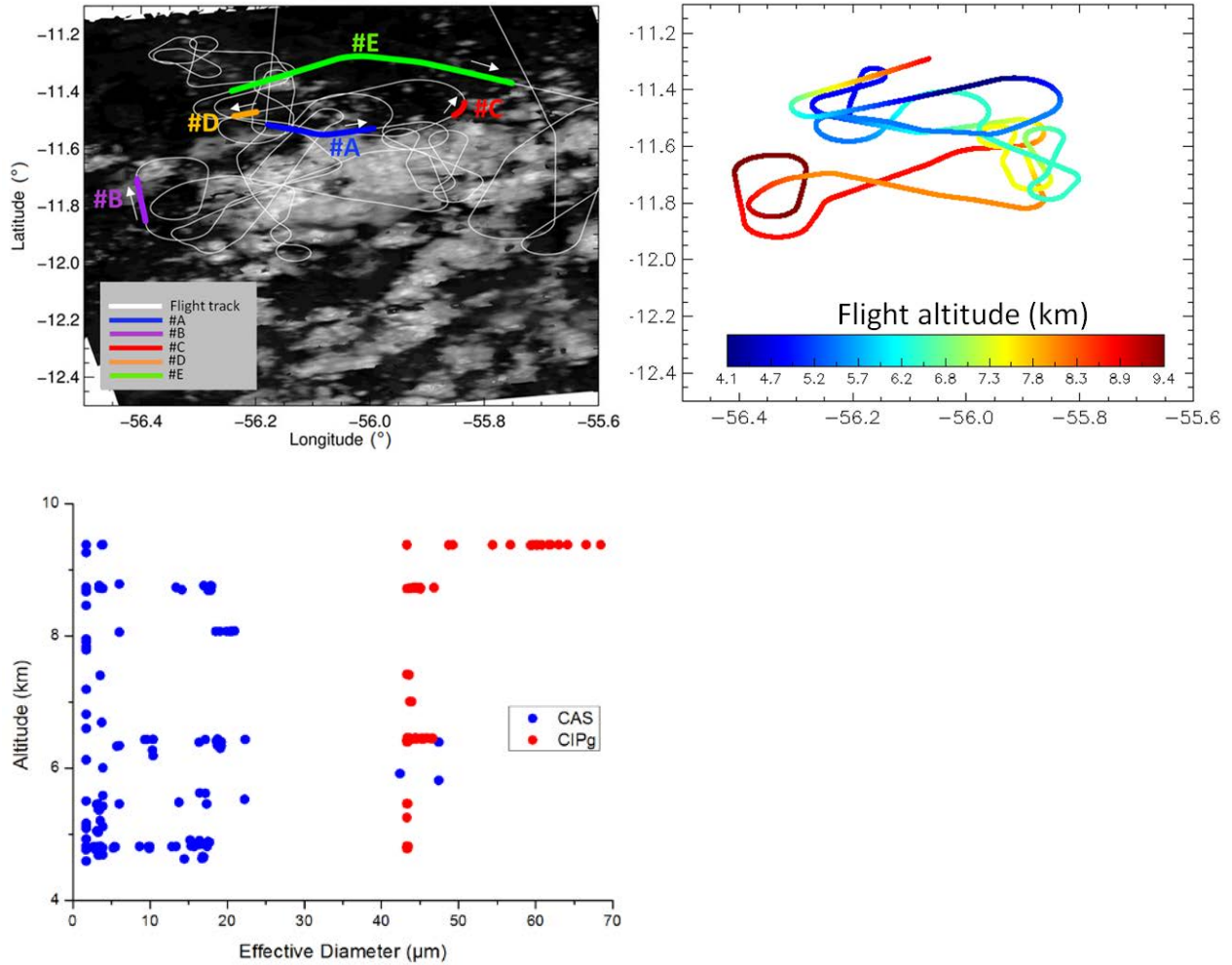
*Page 10: Geometry is Ok, but could be shorter. Except a real 3D cloud structure would be the final product.*

Another publication is in preparation for AMT which will discuss the 3D reconstruction of clouds based on photogrammetry and O2-A band absorption (Zinner et al.).

*Page 12 line 12: A profile and comparison of remote sensing and insitu droplet size would be interesting. A sharp transient of the droplet size shows the transition layer.*

Indeed, a profile of the in situ measured particle size would be interesting. But in situ measurements have the disadvantage that they provide only data along the flight path. As we see from the satellite picture, a large cluster was probed during AC13. The flight altitude is color coded in the right panel (see plot below). From this flight pattern no profile of a single cloud is available, because the flight altitude varied over a large area comprising different clouds of different evolution stages in the cluster.

A combined profile of the effective particle diameter is shown below. The data are based on measurements of the CAS-DPOL and CIPg (Cloud Imaging Probe grayscale, size range: 15 to 960  $\mu\text{m}$ , operated by Mainz University). A distinct increase of the particle size cannot be observed, neither by the CIPg, nor by the CAS-DPOL (size range < 50  $\mu\text{m}$ ).

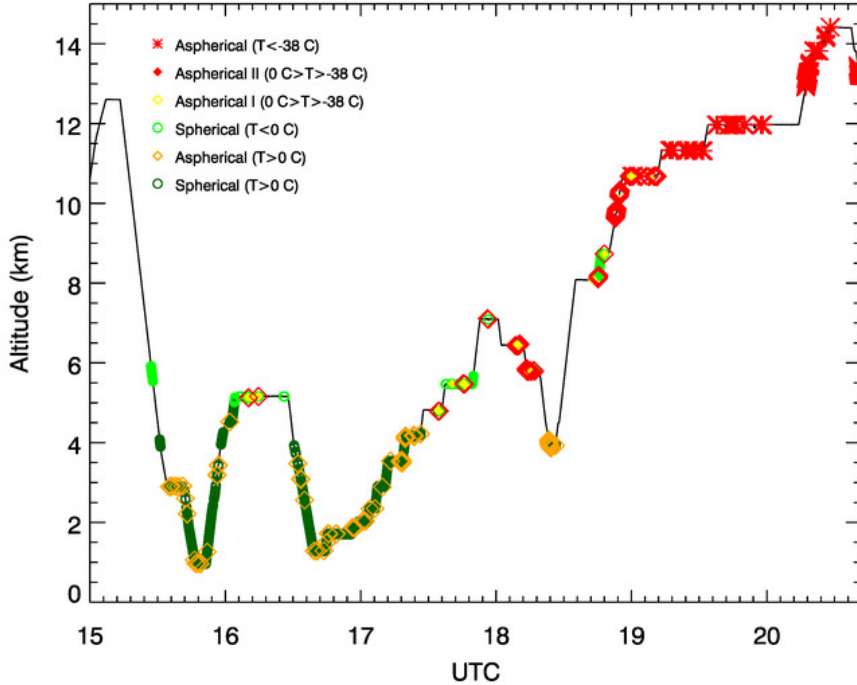


Page 12 line 30: mixed phase levels → phase transition levels or better layer

Fully developed deep convective clouds with cloud tops between 10 and 14 km (classified as ice cloud) and low level cumulus clouds up to 6 km (liquid water clouds) are detected. Cloud phase information from the assumed phase transition layers is not available in Collection 6.

Page 13 line 20: Why are liquid water data from up to 8.7 km not shown

We didn't show the time series of the NIXE-CAPS data for AC18 as a separate plot as provided for AC13. The phrase "not shown" is removed from the text. In case the reviewer is interested in the time series, please find the plot of the data below:



Page 14 line 2: A temp profile is missing.

Fig. 10 also includes a secondary y axis illustrating the temperature as vertical coordinate.

Page 14 line 25: three phases?

The sentence was changed as follows:

Depending on the viewing geometry and cloud distance, layers of pure liquid and ice phase, as well as phase transition layers were identified.

Page 14 line 29: Is there only one polluted case during the whole campaign?

Cecchini et al., (2017) have listed the characteristics of the flights illustrating the aerosol conditions:

**Table 1:** General characteristics of the cloud profiling missions of interest to this study: condensation nuclei ( $N_{CN}$ ) and CCN concentrations ( $N_{CCN}$ , with  $S = 0.48\% \pm 0.033\%$ ), cloud base and 0 °C isotherm altitude ( $H_{base}$  and  $H_{0^\circ C}$ , respectively), start and end time and total number of DSDs collected. The data are limited to the lower 6 km of the clouds. The unit for  $N_{CN}$  and  $N_{CCN}$  is  $\text{cm}^{-3}$  and the unit for altitudes is in m. Profile start and end are given in local time.

Region	Flight	$N_{CN}$ ( $\text{cm}^{-3}$ )	$N_{CCN}$ ( $\text{cm}^{-3}$ )	$H_{base}$ (m)	$H_{0^\circ C}$ (m)	Start	End	# DSDs
Atlantic Coast	AC19	465	119	550	4651	13:17	14:57	630
Remote	AC09	821	372	1125	4823	11:30	14:21	665
Amazon	AC18	744	408	1650	4757	12:32	14:14	397
Arc of Deforestation	AC07	2498	1579	1850	4848	13:49	17:16	674
	AC12	3057	2017	2140	4938	12:55	15:16	381
	AC13	4093	2263	2135	4865	12:46	15:36	204

AC13 was the most promising flight to measure polluted conditions with the largest number of condensation nuclei. For AC12 most of the flight was performed at flight altitude below 6 km, therefore no deep convective clouds have been observed by specMACS.

*Page 14 line 30 bottom: Low statistics? Are those 2 flights analysed in this study the only possible ones of the whole campaign?*

From the 14 scientific flights we selected the three days (AC10, AC13, and AC18) with the best conditions as stated in beginning of Sect. 4:

- (i) no cloud layer above the observed cloud (no cirrus), which contaminates the spectral signature,
- (ii) high proportion of illuminated cloud parts in the vertical direction of the cloud,
- (iii) flight altitude that allows measurements of an extended vertical region of the cloud considering the limited FOV of specMACS, and
- (iv) isolated clouds with recognizable structures for cloud geometry retrievals.

This limits the number of cases. Similar limitations are also reported for the in situ data sampling as shown in Costa et al., (2017). They had data from cloud passages lasting between 1 and 18 minutes in sum per flight.

## Reply to Reviewer #2:

We thank the reviewer for the time and efforts she/he spent reading our manuscript and providing valuable suggestions and advices. Please find below a discussion of the reviewer's comments (*italic*). Changes/additions made to the text are underlined and given in quotes.

The general comments made by the reviewer summarize the main points of the specific comments and suggestions. Therefore, we will start with our replies on the specific and sequential comments.

*p3,L5: I don't see the relevance of the cited paper (Cahalan, 1994) and the associated science (plane-parallel retrieval assumptions) in this context.*

Since the profile retrieval of the cloud phase from MODIS as applied later is based on the cloud particle size retrieval, we included here also the limitations of the size retrieval with respect to the bias caused by 1D assumptions. However, we removed parts of the text and added the following:

From the ensemble of retrieved effective droplet sizes, a vertical profile of cloud phase can be estimated because of the relationship between cloud phase and vertical profile of the cloud particle size (Rosenfeld and Feingold, 2003; Yuan et al., 2010; Martins et al., 2011). However, the retrieval of the effective droplet size relies on one-dimensional (1D) radiative transfer simulations, which incorporates retrieval uncertainties due to plane-parallel cloud assumptions and neglecting the net horizontal radiative transport between the satellite pixels (Zinner et al., 2006). Consequently, a decrease of pixel size causes an increase of the independent pixel bias, because the smaller the pixel, the more important is the net horizontal photon transport, particularly for the wavelengths in the visible spectral range, which are used for the retrieval of the effective droplet radius.

*p3,L17+L30: These are places where the manuscript could outline how the specific work fits into the larger context that was set up previously. Currently, this page in particular looks like a list of work done by the authors and predecessors (e.g., Martins, Rosenfeld), with only tangential connection to the motivation from the previous page(s). This is not a deal breaker for the manuscript, but it would be better to see how the listed work serves a number of outstanding questions related to the introductory comments earlier on.*

Starting from p2125 a technical and experimental review is given how profiles of the cloud microphysical parameters can be derived. This review is mainly focused on passive remote sensing approaches, either from satellite observations (ensemble method), or aircraft observations but also from ground-based measurements. Data products based on these approaches will be used in this study. Therefore, it is worthwhile to describe them shortly here. Most of the cited literature is related to a technical description of the individual retrieval approaches with no or only less discussion on e.g., aerosol-cloud interaction.

To strengthened the connection between motivation and the presented phase retrieval we added the core questions at the end of the introductions:

In this paper we will address the following questions: (i) Can we observe differences in the vertical distribution of the thermodynamic phase state in DCCs for different aerosol conditions by using cloud side observations? (ii) How do the vertical profiles of cloud phase derived from cloud side observations agree with results from satellite (ensemble method) and in situ measurements?

*p4,L4: In the description of the manuscript's structure, it seems that the goal is to compare remote sensing derived cloud profiles to MODIS and in-situ data, which would make the manuscript more appropriate for AMT than for ACP. If, however, there are some higher-level goals that address some of the questions brought up above, this should be made clearer.*

The manuscript was submitted to be published in a special issue of AMT/ACP presenting results from the ACRIDICON-CHUVA campaign. Admittedly, parts of the manuscript include the description of the applied method, but compared to former publications dealing with cloud side observations, this manuscript presents the results of an entire campaign. We are aware, that the number of cases is limited. From the 14 scientific flights we selected the three days (AC10, AC13, and AC18) with the best conditions as stated in the beginning of Sect. 4:

- (i) no cloud layer above the observed cloud (no cirrus), which contaminates the spectral signature,
- (ii) high proportion of illuminated cloud parts in the vertical direction of the cloud,
- (iii) flight altitude that allows measurements of an extended vertical region of the cloud considering the limited FOV of specMACS, and
- (iv) isolated clouds with recognizable structures for cloud geometry retrievals.

This limits the number of cases. Similar limitations are also reported for the in situ data sampling as shown in Costa et al., (2017). They had data from cloud passages lasting between 1 and 18 minutes in sum per flight.

We adapted the outline of the paper to point out that the retrieval method is applied to different cloud cases under different aerosol conditions and discussed using also other observation strategies.

The variability of vertical phase distribution is discussed with respect to aerosol conditions and compared to in situ and MODIS products.

*p4,section 2.1: A table with flights and clouds cases would help.*

We added a table summarizing the three flights which are presented in this work.

A summary of the three flights used in this work is given in Table 1.

**Table 1.** Summary of presented flights with cloud side observations during the ACRIDICON-CHUVA campaign. The ranges of flight altitude and time refer to the studied cloud cases.

Flight number	AC10	AC13	AC18
Aerosol conditions	moderate	polluted	moderate
AOD (MODIS)	0.4 - 0.5	0.5 - 0.6	0.3 - 0.4
Number of cloud cases	9	16	10
Flight altitude range (km)	7.4 - 10.4	5.2 - 9.3	1.4 - 14.0
Time range (UTC)	17:25 - 19:20	17:55 - 19:00	15:30 - 20:30

*p5,L12-18: The manuscript should elaborate on the stereo algorithm a little more. Also, L21, should this be "assign" instead of "allocate"?*

Please read our response to the commentary on p.10 dealing with the stereo algorithm. Furthermore we changed the sentence as suggested:

This allows assigning elevation and azimuthal angle to each point of the image.

*p6,L23: The description of the aspherical fraction is a bit unclear; what is measured, and what is derived?*

The aspherical fraction from the CAS-DPOL is determined by measuring the perpendicularly polarized light in the backward direction and the forward scattering light intensity. While the forward scattered light intensity is used to determine the size of the particle, the ratio of the forward and the backward scatter light determines the phase of the particle. While spherical particles do not change the polarization ratio, aspherical particles do. In order to categorize into liquid and ice particles, a size dependent threshold was inferred from calibration measurements of spherical liquid particles in the AIDA cloud chamber (Järvinen et al., 2016, Schnaiter et al., 2016). Particles with a polarization ratio larger than the 1-sigma range of the inferred sphericity-threshold were categorized as aspherical. The method gives a size dependent aspherical fraction of the first 300 particles measured each second. The bulk aspherical fraction was derived from the number of aspherical particles to the number of total particles measured between 3 and 50  $\mu\text{m}$  per second.

We condensed it, because the CAS-DPOL principle is similar to that of the NIXE-CAS:

The aspherical fraction (AF) from the CAS-DPOL is determined by measuring the perpendicularly polarized light in the backward direction and the forward scattering light intensity. The ratio of the forward and the backward scattered light determines the phase of the particle. Particles with a polarization ratio larger than the 1-sigma range of the inferred sphericity-threshold are categorized as aspherical. The method gives a size dependent aspherical fraction of the first 300 particles measured each second. The bulk aspherical fraction is derived from the number of aspherical particles to the number of total particles measured between 3 and 50  $\mu\text{m}$  per second.

*p6,L30: Why is the threshold this high? 0.3 g/m<sup>3</sup> seems excessive, considering that a typical BL cloud top-level LWC is 1 g/m<sup>3</sup>.*

We added the following:

The Hotwire sometimes returns a signal in ice or clouds of partly frozen particles. This signal is on the order of 0.2 g m<sup>-3</sup>. Thus a conservative threshold of 0.3 g m<sup>-3</sup> is used to reduce the false alarm rate.

*p7,I1: Why is it necessary to perform 3D calculations? Only because of the geometry, or because deviations from standard 1D models are expected? If so, what are they (aside from shadows)*

A convenient way to simulate cloud side reflections is to use 3D radiative transfer models, where the geometry of the observation strategy can be directly transferred to the model setup. There are ways to use 1D radiative transfer simulations instead by adapting the viewing and zenith angle. But this underlies restrictions, because no horizontal transport can be considered. This was shortly discussed in Marshak et al. (2006) and Martins et al. (2011). With respect to 3D radiative effects, less impact due to shorter photon paths is observed for absorbing wavelengths as were used for the phase retrieval. However, at cloud edges with lower optical thickness ( $\tau < 30$  after Martins et al., 2011) the cloud reflection at cloud particle absorbing wavelengths is still variable, but gets saturated starting from  $\tau = 40$  (Marshak et al., 2006). Summarized, with some limitations the phase indices could be also derived by plane parallel simulations. But in any case considering cloud shadow effects (as in section cloud masking procedure) 3D simulations were necessary.

*p7,16: Rayleigh scattering → molecular scattering?*

We use the term “Rayleigh scattering” (as used in Bodhaine et al., 1999) because it describes the scattering on atoms and molecules.

*p9: Here it becomes quite difficult to understand what the authors are after - the position/width of the mixed layer? Is that the purpose of the simulations? Are they done to only replicate the earlier study, or are they something new?*

We hopefully introduced the purpose of the simulations better now:

In the following, results from radiative transfer simulations using MCARATS are presented. The viewing geometry and the atmospheric description were adapted to the conditions during ACRIDICON-CHUVA on 19 September 2014. These simulations were performed to demonstrate that ice and liquid water phase can be separated from the transition layer under different conditions similar to the results reported by Jäkel et al. (2013). Note, that due to the different viewing geometry, also a different angular range of the scattering phase function was observed than for ground-based measurements. This might have an effect on the characteristics of phase index profile in particular with respect to separation of the mixed phase layer.

*p10: The geometry retrieval description is rather cryptic. Would it help to cite work related to MISR, or is the method unrelated? What happens if the cloud moves during two consecutive images (used for the stereo method)? Also, elaborate on p10,118-19, and state with respect to which coordinate system the “elevation angle” is provided.*

We omitted a detailed description of the method because it includes a lot of equations which are given elsewhere. But for better understanding we referred to a publication which discussed the mathematics for a similar experimental setup (Biter et al., 1983):

The theoretical background on photogrammetry is given in Hartley and Zisserman (2004), while Hu et al. (2009) applied these techniques for cloud geometrical reconstruction. The mathematics for the geometry retrieval, as it is used in this study, is based mainly on the method described by Biter et al. (1983). They deployed a side-looking camera onboard of an aircraft to detect the position of cloud features, similar to the setup presented in this work.

And later:

After coordinate transformation, trigonometric methods (Biter et al., 1983) are applied to calculate the distance between the camera positions P1 and P2 to the observed point C.

We added also a short comment on the meaning of the “elevation angle”:

Repeating this procedure for a number of points yields a relation between elevation angle and cloud height. Note, that the elevation angle represents the elevation angle of the selected tie point of the camera image after correction based on the aircraft attitude data. It basically gives the elevation angle above or below the flight altitude.

We are aware that cloud movement might introduce an additional uncertainty. Therefore, we tried to reduce the time between two consecutive pictures. The GoPro delivered a movie, such that images from different time intervals can be selected for one cloud scene. All evaluated cloud scenes used data from time intervals less than 10 seconds.

The same tie points are chosen in a second image taken about 10 seconds later. Choosing a short time interval helps to reduce the uncertainty of the method induced by cloud movement.

Note, that another publication is in preparation for AMT which will discuss the 3D construction of clouds based on photogrammetry and O<sub>2</sub>-A band absorption (Zinner et al.).

*p10: Others circumvented the whole (rather difficult) stereo algorithm by including an IR channel. Why was that not done here? Were these measurements simply not available? And why did the authors prefer the more complicated method to the simple IR imager?*

The reviewer makes a good point here to bring up the usage of an IR camera. Unfortunately, we had no IR-camera available for this campaign. But another ground-based campaign is scheduled for September/October in 2017 in the Brazilian rainforest using IR-camera and imaging spectrometers together for cloud side observations.

*p11, Applications section. What is it that the paper seeks to find out? Refer to the main question here, at least at the beginning? This whole section reads a little bit like a listing of results with no specific purpose. Quite surely there is one, and that should be clarified more.*

We reordered the beginning of this section a little bit and introduced this sections with the two main questions of the case study:

From the 14 scientific flights three days (AC10, AC13, and AC18) are selected with the best observation conditions for specMACS, namely: (i) no cloud layer above the observed cloud (no cirrus), which contaminates the spectral signature, (ii) high proportion of illuminated cloud parts in the vertical direction of the cloud, (iii) flight altitude that allows measurements of an extended vertical region of the cloud considering the limited FOV of specMACS, and (iv) isolated clouds with recognizable structures for cloud geometry retrievals.

Phase profiles from AC13 representing polluted aerosol conditions will be compared to the two days with less aerosol pollution. Effects of aerosol conditions on the height and thickness of the mixed phase layer will be investigated. Second, it will be demonstrated how comparable the different observation strategies (cloud side, cloud top and in situ) are.

We restructured the subsections a little bit to separate the two major goals of this sections. At the end of Sect. 4.1 we discussed the comparability of the different observation strategies, while at the end of Sect. 4.2 the aerosol impact on the mixed phase layer is summarized.

Sec. 4.1: see comment referring to p13,L12-14

Sec. 4.2:

From theory, the mixed phase layer is expected to be higher for polluted aerosol conditions than for cleaner aerosol conditions, which can partly be confirmed by comparison of the three cases. We found from cloud side observations, that the lower boundary altitude of the mixed phase layer tends to be higher for polluted conditions (AC13: 6.0 - 6.5 km) than for the moderate case of AC18 (5.6±0.2 km), while the upper boundary is shifted from 6.8±0.2 km (moderate case AC10) to 7.4±0.4 km (polluted case AC13).

*p12: It is a bit unclear what the in-situ measurements really have to offer here if “the direct comparison of in situ and remote measurements is difficult”. Really, the in-situ measurements*

*should serve as validation for the remote sensing, but what do we learn if that doesn't work? Is it still worth using the in-situ data? If the comparison does not work out, what does that mean for the initial hypotheses (if there is one: perhaps a question about the interchangeability of pixel/time mentioned earlier?)*

When introducing the in situ measurements we added the following sentences to specify the ideas behind the comparison of the different observation strategies:

The variability of the mixed phase layer in depth and height within a single cloud cluster shows that the vertical distribution at least at the cloud edges is variable. In situ data are used to investigate if such a variability is also observed in the more inner part of the cloud.

*p13: The in-situ data puts ice higher than remote sensing. Which is right? What do we learn here about the representativeness of satellite data and \*its\* consistency with the aircraft measurements?*

We didn't find much differences between the glaciation heights derived from the ensemble method based on particles sizes from MODIS (9 km) and the estimations from the CAS-DPOL (8.7 km). Both are using a larger sample of data which were averaged over the entire cloud cluster. While the time series of the NIXE-CAPS instrument shows for individual cloud passages a glaciation height of 8.0 km which is in much better agreement with the cloud side observations. An assessment about the comparability is given at the end of this subsection (please see comment p13,L12-14).

*p13,L34 (top): So what phase \*does\* MODIS get for 6km? The shown results are certainly not liquid drops, given the large size.*

It's a good point made by the reviewer. We assume that this second peak might indicate the bottom of the mixed phase layer. We added the following:

From the conceptual model of cloud particle size profiles inside a DCC (e.g., Rosenfeld and Woodley, 2003) it might indicate the bottom of the mixed phase layer, when cloud particle size starts to increase. However, this increase is less pronounced than presented in Rosenfeld and Woodley (2003).

*p13,L12-14: Here we get some potentially important conclusions, which should be expanded an elaborated on. What is the significance of this finding? What can the satellite-based ensemble method do, and what not? Do in-situ and remote sensing observations from the aircraft tell two different stories?*

It's hard to give a general conclusion on the validity of the ensemble method due to the limitations of studied cases. For such a statement another study would be required using data from several measurement campaigns comparing in situ with satellite observations. However, for our data set we can conclude the following:

Comparing the glaciation height from MODIS with NIXE-CAPS in situ data and results from specMACS observations shows a deviation of about 1.0 - 1.5 km between the different retrieval techniques and observation strategies. However, the mean profile over the entire cloud cluster derived from CAS-DPOL measurements exhibited a similar glaciation height (of about 8.7 km) as found from the MODIS data. This shows that the satellite-based ensemble method may be representative for a large cloud field.

But for individual clouds NIXE-CAPS and specMACS measurements have shown lower glaciation heights. The most likely reason is related to the fact that the ensemble method relies on cloud top observations of growing clouds in different stages of evolution. As shown in Fig. 9g mainly particle sizes between 22 and 27  $\mu\text{m}$  were derived indicating that profile is dominated by cloud measurements in mature stage. At this stage the particle phase may be altered by up- and downdrafts within the clouds as was shown in Fig. 9e. This leads to an enhanced horizontal variability of the cloud phase state which cannot be resolved by passive remote sensing from cloud top observations. Another, but minor reason of the discrepancy between ensemble method and NIXE-CAPS / specMACS measurements is related to the retrieval uncertainty of the effective cloud particle radius. While scattering properties are well defined for liquid water particles, they are variable for ice particles due to differing habits and crystal shapes (Eichler et al., 2009). This gets even more complicated for cloud tops where phase transition starts. Additional retrieval uncertainties of the particle size directly contribute to the derived profile of  $r_{\text{eff}}$ .

*p14,l5: Does this explain the discrepancy between in-situ obs and remote sensing?*

We added the following:

Also local strong downdrafts can transport ice particles into lower levels, which will be interpreted as mixed phase layer from the cloud side observation perspective. Due to the horizontal variability of cloud phase inside a cloud cluster for example caused by up- and downdrafts, in situ measurements may only reveal liquid phase particles. A direct comparison between the observation strategies is subject to restrictions because of temporal and spatial variability of cloud properties in convective systems.

*p14,l16/17: distinctive \*change\* in gradient, or simply "significant gradient" (change of gradient is a gradient of a gradient ... )*

Changed as suggested.

*p14,L21: Here the question is again why this was chosen over IR imaging.*

As mentioned already, an IR imager was not available during the campaign.

*p14,L31: Earlier, the authors said that the aircraft measurements are not statistically significant to prove/disprove theory. This statement here is not meant to be the main finding of the manuscript, is it? Wouldn't satellite data be more suitable to put this on a statistical basis? If so, what would then be the purpose of the aircraft measurements? This may be obvious, but it would help the reader to understand this point.*

In this part of the conclusions we summarized the findings of the comparison between the three flights (AC10, AC13 and AC18) with respect to aerosol impact on the mixed phase layer height. Conclusions about the comparability is given later (see reply to comment p15,L13).

For moderate aerosol conditions, only few cases exhibited liquid water, mixed phase, and ice phase, which limited the statistical significance of the comparison with AC13. However, comparing the glaciation heights of AC10 ( $6.8\pm 0.2$  km) and AC13 ( $7.4\pm 0.4$  km) we found an indication of an increase of glaciation height and a decrease of glaciation temperature for polluted aerosol conditions. With respect to the occurrence of first ice particles, the lower boundary of the mixed phase layer was derived with 6.0 - 6.5 km for polluted conditions, whereas for AC18 the altitude was shifted down to 5.5 - 6.0 km, which agrees with theory.

*p15,L38(top): The results from remote sensing and in-situ are not really consistent (as discussed earlier by the authors, and noted by the reviewer).*

This sentence was referring to the comparison between NIXE-CAPS and specMACS measurements. We changed the sentence for clarification:

Consistent results of mixed phase zone levels were found from specMACS and NIXE-CAPS measurements, for the flight AC13 with most individual cloud cases showing pure liquid, mixed phase layer and pure ice phase.

*p15,L13: “invariance of space and time” does not seem an appropriate way to describe the assumptions of the ensemble method. It’s really spatial statistics vs. temporal evolution, isn’t it? Secondly, the manuscript now divulges that it did seek to study the aerosol effect on deep convection - or is this a statement that this was done (by others) using MODIS? Clarification is needed here what was done in the manuscript vs. prior work. Is it fair to say that the manuscript got closer to observational evidence for the validity of the interchangeability of spatial statistics and temporal evolution?*

The reviewer is right when describing the ensemble method assumptions by spatial statistics vs. temporal evolution. But we will use here the term “time-space-exchangeability” as it was named in several other publications (e.g., Lensky & Rosenfeld, 2006, Yuan et al., 2010). The main intention of this is short paragraph was to summarize the results of the ensemble method. It was not intended to study aerosol effects on DCCs on the basis of cloud top observations. We rephrased the first sentence for clarification as follows:

Additionally to in situ and cloud side measurements, the glaciation temperature was derived applying an ensemble method based on MODIS data, which assumes time-space-exchangeability for a cluster of clouds with different states of evolution.

*p15,L13: This seems like a fair statement, but how do we interpret it? For which purposes is the satellite-based method good enough, and for which problems do we need to use airborne or tower-based observations (as later suggested by the authors)?*

We made a final conclusion on this as follows:

It is concluded that the assumed time--space--exchangeability used in the ensemble method can give a simplified picture of the vertical distribution of the phase within a field of convective clouds of different stages of evolution. Particularly, cloud tops where phase transition (from liquid to ice) starts and ends needs to be observed by the satellite to profile the thermodynamic phase. The number of these observations has to be significant, since the particle sizes are averaged over a larger domain. So, in general the ensemble method can give an indication when phase transition arises for the first time. However, for estimation of the cloud phase profile at a later stage of the DCC evolution, in situ and also cloud side remote sensing might be the better observation strategy, when phase distribution is altered for example by up- and downdrafts.

*p2,L17: 1) Why is there a new paragraph? 2) Suggest re-wording “In particular ... ” as “The phase transition ... is especially relevant for ... ” without a preceding indent/new paragraph.*

Changed as suggested:

The phase transition from liquid water to ice is especially is relevant for the development of precipitation.

*p2,L25: remains > remain*

Done.

*P3,L30: "In further development of the scanning ... " Something wrong with the language here and the conclusion of this sentence.*

Changed as follows:

Different from the scanning-point-sensor measurements as presented by Martins et al. (2011), this paper introduces airborne measurements of an imaging spectroradiometer called specMACS (spectrometer of the Munich Aerosol Cloud Scanner, Ewald et al., 2016). These observations were used to derive vertical profiles of the phase state of DCCs during the HALO (High Altitude and Long Range Research Aircraft) campaign ACRIDICON (Aerosol, Cloud, Precipitation, and Radiation Interactions and Dynamics of Convective Cloud Systems) - CHUVA (Cloud processes of tHe main precipitation systems in Brazil: A contribUtion to cloud resolVing modeling and to the GPM (GlobAl Precipitation Measurement)) in 2014 (Wendisch et al., 2016).

*p4,L12: add comma after "September"*

Done.

*p4,L21: The "degree" characters should be superscripts.*

Done.

*p5,L7: "by measuring monochromatic radiation from a monochromator" - revise language?*

Changed as follows:

The spectral characteristics were deduced by using monochromator output at selected wavelengths.

*p8,l17: "inlay" > "inset"?*

Done.

*p9,l31 (top of page) " grid cell in" > "grid cell at"*

Done.

*p9,l2: ranging between > from ... to?*

Changed as suggested.

*p9,l13: What is the "first cloud case"? At this point, the table suggested above would really be helpful.*

The first and the second cloud case are not related with the measured cloud cases which will be presented later in the manuscript. To omit confusion, we called the two cases in this section "cloud scenarios" and modified the introduction of the two scenarios as follows:

Two simplified cloud scenarios with different profiles of cloud effective radius and water content are assumed. In both cases the clouds ranged from 4.0 to 11.0 km altitude with a mixed phase layer between 6.4 and 7.0 km. While the first scenario uses constant values of cloud effective radius ( $r_{\text{eff}} = 20 \mu\text{m}$  for liquid water and ice) and water content ( $0.7 \text{ gm}^{-3}$ ), the second scenario assumes variable profiles of the microphysical parameters. These two cases are chosen to identify effects on the  $I_P$ -profile caused by changes of (i) the phase state itself (scenario 1), and (ii) the cloud particle size and water content (scenario 2).

*p9,l6: "originated" > "originating"?*

Done.

*p9,l8: The phase index is significantly shifted to positive values > either it assumes positive values or not - what is the meaning of "significantly shifted to positive values" How about "shifted to positive values"?*

We rephrased the sentences as follows:

In the mixed phase layer the phase index shows a steep increase to values larger than 0.15. The absolute difference of the phase indices between mixed phase layer and pure ice phase layer is less pronounced than between liquid and mixed phase layer.

*p9,l9: Why "obviously"? Perhaps "apparently"? Meaning unclear.*

We modified it:

This might be caused by the fact that the contribution of ice particles within the mixed phase layer leads to an increased absorption of radiation resulting in an increase of the phase index.

*p9,l14: "related" > "relative"?*

Changed.

*p9,l15: move "also" to after "is"*

Done.

*p9,l20-21: Too hard to understand. Try to improve language.*

Changed as follows:

As concluded in Jäkel et al. (2013), the phase index becomes less variable for a water content of more than  $0.4 \text{ g m}^{-3}$  (variation lower than 7 %). This holds true for most of the DCCs when cloud edges are excluded, which are optically thinner than the inner regions of the cloud.

*p9,l22: "as can be concluded" > how can this be concluded?*

We combined the two sentences as follows:

Less impact is attributed to the change of the sensor elevation angle, since the variability of the phase index with respect to the viewing geometry for each phase state in the first cloud scenario

with fixed cloud microphysics is lower than the variability of  $I_p$  due to the changed cloud properties in the second cloud scenario.

*p10,l1: "showing" > "with"*

Done.

*p10,l2: "need to be taken" > move to right after "images" on l1.*

Changed as follows:

To estimate the distance to the observed cloud element (C) two images from different positions (P1 and P2) with a projection of the observed point in both images need to be taken (C1 and C2, so-called tie points) as illustrated in Fig. 5a

*p10,l2: explain "epipolar plane"*

For easier understanding we removed the two sentences mentioning the "epipolar plane". For the following equations this term is not needed.

*p10,l3: What's the "world" coordinate system?*

A world coordinate system is independent of the camera and aircraft coordinate systems. In fact, the spatial location of the camera/aircraft is given in the world reference system (world coordinate system) with : "The x -and y-axis of the world coordinate system (not shown) are pointed to the east and to the north, respectively, while the z-axis is perpendicular to the x-y plane (pointing upward)." as was stated in the manuscript.

We changed the sentence as follows and added another reference:

The geometric problem comprises three coordinate systems: for the camera, the aircraft, and the world coordinate system (longitude, latitude and altitude) for the observed point C (Biter et al., 1983).

*p10,l6: Usage of the word "exemplarily" seems out of place throughout most of the manuscript. How about "for example"?*

Changed as suggested:

For example, a positive pitch angle of the aircraft ...

Here "exemplarily" was removed from the sentence:

The theoretical background on photogrammetry is given in Hartley and Zisserman (2004), while Hu et al. (2009) applied these techniques for cloud geometrical reconstruction.

In Section 3.1 we changed the sentence as follows:

The procedure is applied for an example cloud scene observed during ACRIDICON-CHUVA from 19 September 2014.

In Section 4.1 we exchanged "exemplarily" by "for example":

For example, a closer look at the asphericity is taken for the time range between 18.28 and 18.34 UTC (Fig. 9e).

*p10,l6-7: Unclear what this means - wrong axis perhaps?*

The sentence is extended as follows:

For example, a positive pitch angle of the aircraft (associated with rotation around the aircraft  $y_a$ -axis) rotates the camera (image) around the camera's  $x_c$ -axis as can be deduced from Fig. 5b.

*p11,L25: 6b: are the distances in km?*

We added the unit in the text:

From stereographic analysis of these tie points the distances to the cloud points (in km) are determined (Fig. 6b).

*p11,L27: "quite \*a\* homogeneous" (add "a")*

Done.

*p11,l14: "scientific" > "science"*

Done.

*p11,l16: "which" > "because it" ?*

Changed as suggested.

*p12,L30 (top): "have been" > "were"*

Done.

*p12,l32 (top): "phase states. Mainly" > "phase states, mainly"*

Done.

*p15,L15: ATTO - introduce acronym somewhere.*

The Amazon Tall Tower Observatory – was already introduced in Section 2.1 Field campaign.

### Reply to Reviewer #3:

We thank the reviewer for the time and efforts she/he spent reading our manuscript and providing valuable advices. Please find below a discussion of the reviewer's comments (*italic*). Changes/additions made to the text are underlined and given in quotes.

*P4, L14: Is humidity variation small for selected 14 flight cases? If not, influence on the conclusions of this paper should be discussed.*

In another publication of the ACRIDICON-CHUVA special issue, Cecchini et al. (2017b) found differences in the cloud base altitudes which are related to the humidity. Deforestation plays a role to explain contrasts between flights in different Amazonian regions. They found less relative humidity (75 %) and a higher cloud base (2000 m) in the southern region (AC13) which is affected by deforestation compared to measurements over the forest in the north (80 % RH and 1500 m cloud base). This results in a 500 m thinner warm layer for the polluted cloud. Since we didn't measure the humidity at cloud base during the entire time frame of the specMACS cloud side observations, it is difficult to a relation between humidity and cloud evolution in this work. Therefore, we refer to the paper of Cecchini et al. (2017b) where other cloud cases also from other flight days where discussed.

We added the following:

The temperature profiles of the three flights show only small day-to-day variations in spite of the different flight directions. In contrast, the relative humidity is variable with flight area and altitude as was shown by Cecchini et al. (2017b). They discussed in particular the relation between cloud base and humidity below clouds for several flights performed during the ACRIDICON-CHUVA campaign. For AC13 they found less relative humidity (75 %) and a higher cloud base (2000 m) due to deforestation than compared to measurements over the rain forest (80 % relative humidity and 1500 m cloud base).

*Subsection 2.2.2 (MODIS) should be moved to after Subsection 2.2.4 (CAS-DPOL...) because Subsections 2.2.1, 2.2.3 and 2.2.4 describe the aircraft measurements.*

The original intention of the order was to separate remote sensing and in situ instruments. However, we changed the order of chapters as suggested by the reviewer.

*P5, L25: The MODIS thermodynamic phase algorithm should be explained in more detail for better discussion (around P12, bottom) on the comparison of aircraft measurement results with the MODIS phase results.*

We introduced the retrieval of the cloud top phase as provided by the MYD06 data set in more detail and gave some more references. Now it is clearly stated, that with the latest Collection 6, the "mixed phase" class is now combined with the "uncertain" class, in order that a separation of cloud tops with only mixed phase cannot given.

Since MODIS mainly measures cloud top properties, the timespaceexchangeability of convective clouds as proposed by Rosenfeld and Lensky (1998) is applied and referred to as ensemble method. The cloud particle phase of the cloud tops is directly taken from the MOD06/MYD06 20 product "Cloud Phase Infrared" with a 1-km-pixel resolution (Baum et al., 2012). Compared to Collection 5, where the cloud phase product was classified as ice, liquid water, mixed phase, and uncertain using brightness temperatures measured at 8.5

and 11  $\mu\text{m}$  (Platnick et al., 2003), Collection 6 is modified by using additional cloud emissivity ratios (7.3/11, 8.5/11, and 11/12  $\mu\text{m}$ ) as reported by Pavolonis (2010) and Baum et al. (2012). Empirically derived thresholds of these emissivity ratios were defined to separate finally between liquid water and ice clouds. Note, that due to ambiguity reasons (see Platnick et al. (2017)) a separate classification of mixed phase cloud pixels is no longer provided in Collection 6. The "mixed phase" and "uncertain" classes from Collection 5 are now combined into a single class specified as "undetermined". Hence, the description of the cloud phase profile by applying the ensemble method on the "Cloud Phase Infrared" product is limited to the liquid water and the ice phase distribution. Therefore, the cloud particle size product is used additionally to estimate the glaciation temperature as proposed by Yuan et al. (2010).

The description of the phase statistics as derived from the cloud top and phase frequency plot was modified as follows:

In Fig. 9f the frequency of liquid and ice phase observations for altitude bins of about 200 m is presented. Fully developed deep convective clouds with cloud tops between 10 and 14 km (classified as ice cloud) and low level cumulus clouds up to 6 km (liquid water clouds) are detected. Cloud phase information from the assumed phase transition layers is not available in Collection 6.

And later:

The MODIS phase product shows ice cloud tops between 11 and 15 km altitude and liquid water clouds up to 4.5 km.

*P6, L24, "The aspherical fraction is the ratio of aspherical particles ... ": Is this a ratio of number concentration? Other definitions (area, volume, or mass) of the ratio are possible. Please clarify the definition.*

We specified the definition as follows:

The aspherical fraction (AF) is determined by a size dependent ratio of the polarized backward scattered and the forward scattered light with respect to their number concentration.

*P14, L4, the last sentence of this Subsection, "Also strong downdrafts can ... ": The last part of this sentence, "whereas in situ measurements inside the cloud only reveal liquid phase particles", is confusing to me. Why do cloud side observation and in situ measurements show different results?*

As in situ and cloud side measurements are not collocated in time and space one of the main reasons is the horizontal variability of cloud properties which causes differences in the determination of the cloud phase. This variability is enhanced for increasing vertical velocity within the clouds. We modified the paragraph as follows:

Also local strong downdrafts can transport ice particles into lower levels, which will be interpreted as mixed phase layer from the cloud side observation perspective. Due to the horizontal variability of cloud phase inside a cloud cluster for example caused by up- and downdrafts, in situ measurements may only reveal liquid phase particles. A direct

comparison between the observation strategies is subject to restrictions because of temporal and spatial variability of cloud properties in convective systems.

Typographic corrections

*P9, L32, "140 x 40 x 99": The "x" character should be replaced by the times symbol.*

Done. Also exchanged at other places.

*P9, L20, "get": Should be replaced by "become" or something.*

Done.

*P12, L22, "m s<sup>-1</sup>": Make the "-1" superscript.*

Done.

# Vertical distribution of the particle phase ~~state of particles~~ in tropical deep-convective clouds as derived from cloud-side reflected solar radiation measurements

Evelyn Jäkel<sup>1</sup>, Manfred Wendisch<sup>1</sup>, Trismono C. Krisna<sup>1</sup>, Florian Ewald<sup>2,3</sup>, Tobias Kölling<sup>2</sup>, Tina Jurkat<sup>3</sup>, Christiane Voigt<sup>3</sup>, Micael A. Cecchini<sup>4</sup>, Luiz A. T. Machado<sup>4</sup>, Armin Afchine<sup>5</sup>, Anja Costa<sup>5</sup>, Martina Krämer<sup>5</sup>, Meinrat O. Andreae<sup>6,7</sup>, Ulrich Pöschl<sup>6</sup>, Daniel Rosenfeld<sup>8</sup>, and Tianle Yuan<sup>9</sup>

<sup>1</sup>Leipzig Institute for Meteorology (LIM), University of Leipzig, Germany.

<sup>2</sup>Meteorological Institute, Ludwig-Maximilians-University Munich, Germany.

<sup>3</sup>Institut für Physik der Atmosphäre, Deutsches Zentrum für Luft und Raumfahrt (DLR), Oberpfaffenhofen, Germany.

<sup>4</sup>Center of Weather Forecast and Climates Studies (CPTEC), National Institute for Space Research (INPE), Sao Jose Dos Campos, Brazil.

<sup>5</sup>Forschungszentrum Jülich, Jülich, Germany.

<sup>6</sup>Max Planck Institute for Chemistry (MPIC), Mainz, Germany.

<sup>7</sup>Scripps Institution of Oceanography, University of California San Diego, La Jolla, California, USA.

<sup>8</sup>Institute of Earth Sciences, The Hebrew University of Jerusalem, Jerusalem, Israel.

<sup>9</sup>NASA Goddard Space Flight Center, Greenbelt, Maryland, USA.

*Correspondence to:* E. Jäkel  
e.jaekel@uni-leipzig.de

**Abstract.** Vertical profiles of the cloud particle phase state in tropical deep-convective clouds (DCCs) were investigated using airborne solar spectral radiation data collected by the German ~~research aircraft HALO~~ High Altitude and Long Range Research Aircraft (HALO) during the ACRIDICON-CHUVA campaign, which was conducted over the Brazilian ~~Amazon rainforest~~ in September 2014. A phase discrimination retrieval based on imaging spectroradiometer measurements of ~~cloud-DCC~~ side spectral reflectivity was applied to ~~DCCs under clouds formed in~~ different aerosol conditions. From the retrieval results the height of the mixed phase layer of the DCCs was determined. The retrieved profiles were compared with in situ measurements and satellite observations. It was found that the depth and vertical position of the mixed phase layer can vary up to 900 m for one single cloud scene. ~~In particular, this variation~~ This variability is attributed to the different stages of cloud development in ~~one a~~ scene. Clouds of mature or decaying stage are affected by falling ice particles resulting in lower levels of fully glaciated cloud layers compared to growing clouds. Comparing polluted and moderate aerosol conditions revealed a shift of the lower boundary of the mixed phase layer from  $5.6 \pm 0.2$  km (269 K) [moderate] to  $6.2 \pm 0.3$  km (267 K) [polluted], and of the upper boundary from  $6.8 \pm 0.2$  km (263 K) [moderate] to  $7.4 \pm 0.4$  km (259 K) [polluted], as would be expected from theory.

## 1 Introduction

Deep-convective clouds (DCCs) play a crucial role in redistributing latent heat, influencing the hydrological cycle, and regulating the radiative energy budget of the Earth's climate system. In particular, tropical convection is a key component of the global circulation of the atmosphere, which is the primary pathway for energy transport from the tropics to the mid-latitudes.

5 DCCs exhibit a ~~highly~~ high variability of cloud particle sizes and a complex vertical microphysical structure, ~~including~~. This includes the different phase states of water (liquid ~~, mixed phase,~~ and ice) ~~and a high variability of cloud particle sizes of the~~ cloud particles and the occurrence of layers where phase transitions between liquid water and ice particles (further referred to as mixed phase) take place. The optical, microphysical, and macrophysical properties of DCCs determine their radiative effects and are controlled by particle growth ~~processes~~ occurring within the clouds.

10 Consequently, the understanding of the processes driving the evolution of DCCs is of major importance. In particular, aerosol particles modify cloud properties, including their radiative effects (Twomey, 1977), as well as their lifetime and the formation of precipitation (Albrecht, 1989). Many efforts have been undertaken to quantify these effects ~~and processes~~, which take place over a wide range of spatial and temporal scales (Rosenfeld et al., 2014). Aerosol particles have an influence on the cloud droplet size distributions (more ~~aerosols~~ aerosol particles lead to more and smaller cloud droplets), on warm rain and cold rain

15 development, on the cloud top height evolution, the depth of the mixed phase layer, and the occurrence of lightning (Tao et al., 2012). While the formation of ~~warm-rain~~ warm rain is suppressed by enhanced aerosol particle number concentration, the cold-rain evolution is intensified due to extra latent heat, which leads to an invigoration of the DCC development (Andreae et al., 2004; Rosenfeld et al., 2008). ~~In particular, the~~ The phase transition from liquid water to ice is especially relevant for the development of precipitation. Furthermore, the optical properties of ice and liquid water clouds differ and ~~thus cause different~~, thus, cause variable radiative effects. Rosenfeld and Lensky (1998) found that in continental clouds glaciation occurs at much colder temperatures ( $-15^{\circ}\text{C}$  to  $-30^{\circ}\text{C}$ ) than in maritime clouds (warmer than  $-10^{\circ}\text{C}$ ). Consequently, the vertical transitional mixed phase zone in continental clouds is geometrically thicker than in maritime clouds. In polluted clouds the coalescence zone vanishes (in which droplet growth by collision and coalescence play a major role), and mostly small liquid water droplets are observed. The mixed phase zone is shifted to lower temperatures (less than  $-15^{\circ}\text{C}$ ), and glaciation occurs often above the

25  $-30^{\circ}\text{C}$  isotherm, with the extreme situation of polluted clouds with strong updrafts reaching to  $-38^{\circ}\text{C}$  (Rosenfeld and Woodley, 2000).

Profile measurements of microphysical structure and formation of precipitation ~~remains~~ remain a challenge. Either in situ measurements (Freud et al., 2008; Konwar et al., 2012; Khain et al., 2013, e.g.,) or remote sensing techniques are applied to obtain profiles of cloud microphysical parameters, such as cloud particle size and phase state. Active remote sensing ~~measurements~~

30 observations (e.g., radar) provide profiles along the line-of-sight. These sensors may penetrate through a cloud, but the quantitative retrieval of cloud optical and microphysical properties is problematic since the signal is dominated by scattering due to large droplets.

Rosenfeld and Lensky (1998) introduced a method to derive vertical profiles of the effective droplet radius as a function of brightness temperature from satellite reflectance measurements. They analyzed clusters of convective clouds at different stages

of vertical development to retrieve the temporal evolution of individual cloud elements. This ensemble method assumes that cloud-top properties derived from clouds at different stages of their evolution are ~~similar-comparable~~ to the properties of ~~a single-an individual~~ cloud as it ~~grows-evolves~~ through the various heights (Freud et al., 2008). ~~Rosenfeld et al. (2014) have shown an improved detection of cloud microphysical processes for the 375-m resolution data of the NPP/VIIRS (National Polar-orbiting Partnership/Visible Infrared Imaging Radiometer Suite) compared to the standard 1-km resolution data of MODIS (Moderate Resolution Imaging Spectroradiometer). Small scale convective cloud elements are better resolved with higher spatial resolution by the NPP/VIIRS, whereas MODIS retrievals based-~~From the ensemble of retrieved effective droplet sizes, a vertical profile of cloud phase can be estimated because of the relationship between cloud phase and vertical profile of the cloud particle size (Rosenfeld and Feingold, 2003; Yuan et al., 2010; Martins et al., 2011). However, the retrieval of the effective droplet size relies on one-dimensional (1D) radiative transfer simulations ~~are biased by the-~~, which incorporates retrieval uncertainties due to plane-parallel ~~assumptions (Cahalan, 1994). A cloud assumptions and neglecting the net horizontal radiative transport between the satellite pixels (Zinner et al., 2006). Consequently, a~~ decrease of pixel size causes an increase of the independent pixel bias, because the smaller the pixel, the more important is the net horizontal photon transport-, particularly for the wavelengths in the visible spectral range, which are used for the retrieval of the effective droplet radius.

The retrieval uncertainty due to the 1D approximation and the assumptions made with respect to the ensemble method can be mitigated by using multi-angle spectroradiometer measurements (ground-based, airborne, or satellite) of cloud side spectral reflectivity ~~to derive vertical profiles of microphysical cloud parameters~~. A step further is the application of high-resolution imaging spectroradiometers, which ~~offer a~~ enables profiling of individual clouds with a temporal resolution of one minute from both ground or aircraft. For airborne applications there are no safety-related flight restrictions due to strong turbulences and icing as would be required in case of cloud penetrations for in situ probing.

The retrieval approach of the thermodynamic water phase based on cloud side observations exploits the differences in the imaginary part of the refractive index of the cloud particles of both phases in the near infrared (NIR: 0.7-2.5  $\mu\text{m}$ ) wavelength range (Pilewskie and Twomey, 1987; Ehrlich et al., 2008; Martins et al., 2011; Jäkel et al., 2013). While Pilewskie and Twomey (1987) and Jäkel et al. (2013) applied ground-based measurements of spectral reflectivity between 1.5 – 1.7  $\mu\text{m}$  wavelength for the phase discrimination, Martins et al. (2011) and Marshak et al. (2006) utilized reflected radiation data at 2.10  $\mu\text{m}$  and 2.25  $\mu\text{m}$  wavelength. A phase index was defined by Jäkel et al. (2013) using the spectral slope of cloud side reflected radiances between 1.55 and 1.7  $\mu\text{m}$ . ~~They~~ Jäkel et al. (2013) showed by applying three-dimensional (3D) radiative transfer simulations that this slope is negative for liquid water and positive for ice particles, mostly independent of the viewing geometry and cloud particles size. For DCCs with liquid water, ice particles, and mixed phase layers, profile measurements of the phase index provide evidence where and in which stage of development ice particles start to form. For ground-based observations, Jäkel et al. (2013) identified the mixed phase zone by a strong increase of the phase index from negative to positive values, while the vertical profile of the phase index for pure liquid water or ice particles is less variable.

To determine the height and temperature of the mixed phase layer from cloud side spectral reflectivity observations additional information is required. Martins et al. (2011) used a thermal infrared sensor at 11  $\mu\text{m}$  wavelength yielding the brightness temperature, which is an indicator of cloud height. Collocated scanning active remote sensing techniques by radar or lidar were

applied to estimate geometric information on cloud distance and height (Jäkel et al., 2013; Ewald et al., 2015). Another method is based on stereographic analysis of multiangle observations (e.g., Seiz and Davies, 2006).

~~In further development of the scanning, point-sensor~~ Different from the scanning-point-sensor measurements as presented by Martins et al. (2011), this paper introduces airborne measurements of an imaging spectroradiometer called specMACS (spec-

5 ~~trometer of the Munich Aerosol Cloud Scanner, Ewald et al., 2016)~~ to characterize. These observations were used to derive vertical profiles of the phase state of DCCs ~~as observed~~ during the HALO (High ~~L~~Atitude and ~~L~~ong-range research aircraft Altitude  
and Long Range Research Aircraft) campaign ACRIDICON (Aerosol, Cloud, Precipitation, and Radiation Interactions and  
Dynamics of Convective Cloud Systems) - CHUVA (Cloud processes of tHe main precipitation systems in Brazil: A contri-  
bUtion to cloud resolVing modeling and to the GPM (GlobAl Precipitation Measurement)) in 2014 (Wendisch et al., 2016).

10 The measurement technique of imaging spectroradiometers allows instantaneous spectral cloud side observations for a set of  
viewing angles depending on the number of spatial pixels of the sensor. The imaging spectroradiometer measurements were  
supplemented by GoPro-video camera observations to estimate the cloud distance and height from stereographic analysis ~~of the~~  
additional video-camera data.

In this paper we will address the following questions: (i) Can we observe differences in the vertical distribution of the  
15 thermodynamic phase state in DCCs for different aerosol conditions by using cloud side observations? (ii) How do the vertical  
profiles of cloud phase derived from cloud side observations agree with results from satellite (ensemble method) and in situ  
measurements?

The instrumentation and the field campaign are introduced in Section 1, followed by a description of the methodology of the  
phase retrieval (See-Section 2). In Section 3 the method is applied to data from three flights conducted during ACRIDICON-  
20 CHUVA. The variability of vertical phase distribution is discussed with respect to aerosol conditions and compared to in situ  
and MODIS-satellite products.

## 2 Measurements and tools

### 2.1 Field campaign

Remote-Airborne remote sensing and in situ data sampled during ACRIDICON-CHUVA are used to derive vertical profiles  
25 of the thermodynamic ~~water-phase-phase~~ phase (ice or liquid water) of cloud particles in DCCs as measured over the Brazilian  
rainforest. Local convection is strongly forced by the diurnal cycle. In particular, at the end of the dry season (September),  
a large variability of aerosol particles due to biomass burning is observed (Andreae et al., 2015). Three out of fourteen scientific  
flights ~~were~~ (labelled as AC10, AC13, AC18) are selected for this study (flight tracks shown in Fig. 1) covering an area of  
about 1400 ~~x-x~~ 1200 km<sup>2</sup>. The temperature profiles of the three flights show only small day-to-day variations in spite of  
30 the different flight directions. In ~~the contrast, the relative humidity is variable with flight area and altitude as was shown by~~  
Cecchini et al. (2017b). They discussed in particular the relation between cloud base and humidity below clouds for several  
flights performed during the ACRIDICON-CHUVA campaign. For AC13 they found less relative humidity (75 %) and a  
higher cloud base (2000 m) due to deforestation than compared to measurements over the rain forest (80 % relative humidity

and 1500 m cloud base). In the overview paper of the ACRIDICON-CHUVA campaign by Wendisch et al. (2016) the aerosol conditions from AC13 was classified as polluted. ~~?~~ Cecchini et al. (2017a) used the aerosol concentration measured with a condensation particle counter (CPC) at cloud base for flights AC13 and AC18 as indicator. They found 4100 particles  $\text{cm}^{-3}$  for AC13 suggesting polluted clouds and about 740 particles  $\text{cm}^{-3}$  for AC18 indicating clouds under Amazonian background conditions typical of the dry season. No appropriate measurements at cloud base ~~were~~ are available for AC10. Ground-based measurements on this day at the Amazonian Tall Tower Observatory (ATTO) located at  $-2.143^{\circ}\text{S}$  and  $-59.001^{\circ}\text{W}$  revealed a particle concentration between 1100 and 1600  $\text{cm}^{-3}$ . Since the flight AC10 was in the same general region, these data are used to describe the aerosol condition of AC10. Furthermore, the aerosol optical depth in the main measurement areas taken from MODIS (Moderate-resolution Imaging Spectroradiometer) product MOD04/MYD04 (3-km-pixel resolution) ~~was~~ are chosen as additional parameter. Quite variable values between 0.3-0.4 for AC18 (28 September 2014), between 0.4-0.5 for AC10 (12 September 2014) and between 0.5-0.6 for AC13 (19 September 2014) ~~were~~ are found. From these data AC10 and AC18 ~~were~~ are classified as moderate aerosol cases. A summary of the three flights used in this work is given in Table 1.

## 2.2 Instrumentation

### 2.2.1 specMACS and GoPro

15 The imaging spectroradiometer specMACS (Ewald et al., 2016) consists of two line cameras (manufactured by SPECIM, Finland), one for the visible and near-infrared (VNIR), the other for the shortwave infrared (SWIR) spectral range. The field of view (FOV) along the spatial lines of both cameras differs slightly ( $33^{\circ}$  and  $35^{\circ}$ ) due to different optics. The incoming solar radiation is distributed over 1312 and 320 spatial pixels, ~~respectively~~. For each spatial pixel, spectral information can be measured within  $0.4 - 1.0 \mu\text{m}$  (800 spectral channels) and  $1.0 - 2.5 \mu\text{m}$  (256 spectral channels), ~~respectively, with a spectral~~ with  
20 a bandwidth between  $2.5 - 12.0 \text{ nm}$ .

~~The measurement system SpecMACS~~ was characterized in the laboratory with respect to nonlinearity, dark current, and polarization (Ewald et al., 2016). Spatial calibrations were performed to derive the angular resolution of both sensors, which is needed for final geometric matching of both sensors. The spectral characteristics were deduced by ~~measuring monochromatic radiation from a monochromator~~ using monochromator output at selected wavelengths. The absolute radiometric response was  
25 determined using an integrating sphere and the absolute RAdiance STAndard (RASTA; Schwarzmaier et al., 2012) traceable to absolute radiance standards of PTB (Physical Technical Bundesanstalt). ~~Finally, The~~ wavelength-dependent uncertainties ( $2\sigma$ ) of the absolute radiometric response including sensor noise and dark current drift between 3 % and 14 % (in the outer region of the measured spectra) were given in Ewald et al. (2016).

During the ACRIDICON-CHUVA campaign, specMACS was mounted at ~~the a~~ side view port on HALO. The transmission of  
30 the optical window with purified quartz glass panes (type: Herasil 102) was characterized in the laboratory. The line cameras were orientated in vertical position as illustrated in Fig. 2. During the aircraft movement 3D (two spatial, one spectral dimension) snapshots of cloud scenes were taken.

For estimates of the cloud distance a two-dimensional (2D) digital action camera (type: Hero HD3+ 3660-023 Full-HD man-

manufactured by GoPro, Inc., USA, and hereafter called GoPro) was installed at the side window of HALO. Movies with full HD at a resolution of 1920 ~~x~~ 1080 pixels were recorded during the flight. The original lens of the camera was replaced by a distortion free optics covering a horizontal  $FOV_h$  of about  $90^\circ$  and a vertical  $FOV_v$  of about  $59^\circ$ . A schematic of the setup is shown in Fig. 2. The geometrical calibration of the camera was performed using a square chessboard. Images from different perspectives of the chessboard were taken and evaluated by an open source routine (<http://opencv.org>) implemented in computer vision algorithms (Bradski and Kaehler, 2013). This allows ~~allocating~~ assigning elevation and azimuthal angle to each point of the image.

### 2.2.2 MODIS

~~MODIS cloud products of the Terra (MOD06) and Aqua (MYD06) satellites have been used in this study for a comparison of the phase state and glaciation temperature. Since MODIS mainly measures cloud top properties, the time-space-exchangeability of convective clouds as proposed by Rosenfeld and Lensky (1998) is applied. The cloud particle phase is directly taken from the MOD06/MYD06 product "Cloud\_Phase\_Infrared" with a 1-km-pixel-resolution (Platnick et al., 2003). The estimation of the glaciation temperature is based on the retrieval presented by Yuan et al. (2010). The vertical distribution and evolution of cloud particle size inside a DCC provides useful information on the phase state (Rosenfeld and Feingold, 2003). The mixed phase layer is characterized by a strong increase of cloud particle size with height, whereas for fully glaciated cloud layers the largest ice particles can be found directly at the height where the glaciation temperature is reached. At lower temperatures, no supercooled droplets are left for particle growth and only small ice particles are able to move upward inside weakened updrafts. Consequently, the height and temperature where the increase of particle size turns into a decrease is considered as glaciation level and temperature. A sufficiently large statistics is required for the ensemble method. The cloud particle sizes from the MOD06/MYD06 product are averaged for a bin of cloud brightness temperatures (Channel 31;  $11 \mu\text{m}$ ). In contrast to the original retrieval (Yuan et al., 2010), the restrictions concerning cloud optical depth ( $COD > 30$ ) and cloud top temperature ( $CTT < 260 \text{ K}$ ) were relaxed to  $COD > 10$  and  $CTT < 280 \text{ K}$ , to enlarge the statistics of the data.~~

### 2.2.2 NIXE-CAPS

In situ measurements of the asphericity of particles were performed with the Novel Ice eXperiment – Cloud, Aerosol and Precipitation Spectrometer (NIXE-CAPS). The instrument is a combination of two probes, the NIXE-CAS (Cloud and Aerosol Spectrometer) and the NIXE-CIP (Cloud Imaging Probe). While the NIXE-CIP detects the size of particles between 15 and  $900 \mu\text{m}$  by recording 2-D shadow cast images, the NIXE-CAS measures the size and asphericity of the particles for a range of 0.6 and  $50 \mu\text{m}$  (Meyer, 2012; Luebke et al., 2016) (Meyer, 2012; Luebke et al., 2016; Costa et al., 2017). NIXE-CAS discriminates between spherical and aspherical particles by measuring the change of the polarized components of the scattered laser light in the backward direction, which is sensitive to the particle shape. Spherical particles ~~do not strongly~~ are not supposed to alter the polarization state of the incident light as discussed by (Meyer, 2012), while non-spherical ice crystals change the polarization depending on ~~the~~ their size and orientation (Nicolet et al., 2007) (Nicolet et al., 2007; Meyer, 2012). With respect to the phase state classification discrimination, aspherical particles can be considered as ice particles. In contrast, spherical par-

ticles indicate mainly liquid droplets. Note, that while Järvinen et al. (2016) have shown that ice particles can also be spherical, the large majority of spherical particles is associated with the liquid phase. The ACRIDCON-CHUVA data set ~~was is~~ classified with respect to temperature, asphericity, and particle number concentration as measured by NIXE-CAPS (see Table 2).

### 2.2.3 CAS-DPOL and LWC hotwire

The CAS-DPOL (Cloud and Aerosol Spectrometer, with detector for polarization) instrument measures aerosol and cloud particles in the size range between 0.5 and 50.0  $\mu\text{m}$  (Braga et al., 2016; ?) (Braga et al., 2016; Voigt et al., 2017) by sensing individual particles passing a focused laser beam. The resulting intensity distribution of forward and backward scattered light is used to derive the size distribution of the particles. ~~Here, only Only~~ particles with diameters between 3 and 50  $\mu\text{m}$  and with a total number density larger than  $1 \text{ cm}^{-3}$  are classified. Additionally, CAS-DPOL is used to estimate the phase of the cloud particles (liquid or ice). The aspherical fraction (AF) ~~from the CAS-DPOL~~ is determined by ~~a size dependent ratio of the polarized backward scattered measuring the perpendicularly polarized light in the backward direction and the forward scattered light. The aspherical fraction is the ratio scattering light intensity. The ratio of the forward and the backward scattered light determines the phase of the particle. Particles with a polarization ratio larger than the 1- $\sigma$  range of the inferred sphericity threshold are categorized as aspherical. The method gives a size dependent aspherical fraction of the first 300 particles measured each second. The bulk aspherical fraction is derived from the number of aspherical particles and the sum of all detected particles to the number of total particles measured between 3 and 50  $\mu\text{m}$  per second.~~ Calibration of the backward channel was performed during RICE03 (Rough ICE campaign) at the AIDA (Aerosol Interactions and Dynamics in the Atmosphere) cloud chamber (Järvinen et al., 2016; Schnaiter et al., 2016). Spherical liquid particles reveal a low AF ( $< 0.1$ ) while aspherical particles (ice or aerosols) have a high AF ( $> 0.1$ , mean of 0.4). Aspherical ice particles may have an AF  $< 1$  since the orientation of the particles in the sampling volume may appear circular.

The liquid water content (LWC) ~~is was~~ measured with a King type LWC Hotwire (Braga et al., 2016) installed on the CAS-DPOL. ~~Only data above a conservative detection limit The Hotwire sometimes returns a signal in ice or clouds of partly frozen particles. This signal is on the order of  $0.2 \text{ g m}^{-3}$ . Thus, a conservative threshold of  $0.3 \text{ g m}^{-3}$  is used to reduce the false alarm rate.~~

### 2.2.4 MODIS

~~MODIS cloud products (Collection 6) of the Terra (MOD06) and Aqua (MYD06) satellites are used for a comparison of the phase state and glaciation temperature. Since MODIS mainly measures cloud top properties, the time-space-exchangeability of convective clouds as proposed by Rosenfeld and Lensky (1998) is applied and referred to as ensemble method. The cloud particle phase of the cloud tops is directly taken from the MOD06/MYD06 product "Cloud Phase Infrared" with a 1-km-pixel resolution (Baum et al., 2012). Compared to Collection 5, where the cloud phase product was classified as ice, liquid water, mixed phase, and uncertain using brightness temperatures measured at 8.5 and 11  $\mu\text{m}$  (Platnick et al., 2003), Collection 6 is modified by using additional cloud emissivity ratios (7.3/11, 8.5/11, and 11/12  $\mu\text{m}$ ) as reported by Pavolonis (2010) and Baum et al. (2012). Empirically derived thresholds of these emissivity ratios were defined to separate finally between liquid~~

water and ice clouds. Note, that due to several ambiguities (see Platnick et al. (2017)) a separate classification of mixed phase cloud pixels is no longer provided in Collection 6. The "mixed phase" and "uncertain" classes from Collection 5 are now combined into a single class specified as "undetermined". Hence, the description of the cloud phase profile by applying the ensemble method on the "Cloud\_Phase\_Infrared" product is limited to the liquid water and the ice phase distribution. Therefore, the cloud particle size product is used additionally to estimate the glaciation temperature as proposed by Yuan et al. (2010). The vertical distribution and evolution of cloud particle size inside a DCC provides useful information on the phase state (Rosenfeld and Feingold, 2003). The mixed phase layer is characterized by a strong increase of cloud particle size with height (Martins et al., 2011), whereas for fully glaciated cloud layers the largest ice particles can be found directly at the height where the glaciation temperature is reached. At lower temperatures, no supercooled droplets are left for particle growth and only small ice particles are able to move upward inside weakened updrafts. Consequently, the height and temperature where the increase of particle size turns into a decrease is considered as glaciation level and temperature. A sufficiently large statistics is required for the ensemble method. The cloud particle sizes from the MOD06/MYD06 product are averaged for a bin of cloud brightness temperatures (Channel 31; 11  $\mu\text{m}$ ). In contrast to the original retrieval (Yuan et al., 2010), the restrictions concerning cloud optical depth ( $\text{COD} > 30$ ) and cloud top temperature ( $\text{CTT} < 260 \text{ K}$ ) were relaxed to  $\text{COD} > 10$  and  $\text{CTT} < 280 \text{ K}$ , to enlarge the statistics of the data.

### 2.3 Radiative transfer model

3D radiative transfer modeling is performed with the forward-propagating Monte Carlo photon-transport model MCARATS (Monte Carlo Atmospheric Radiative Transfer Simulator) (Iwabuchi, 2006). The optical properties (single scattering albedo, extinction coefficient, and phase function) of atmospheric components are pre-defined by the user for each grid cell of the model domain as either horizontally inhomogeneous or homogeneous layers. Profiles of temperature, atmospheric pressure, density, and gases and gas densities are taken from Anderson et al. (1986) have been adjusted by. From a radio sounding from Alta Floresta ( $-9.866^\circ\text{S}$ ,  $-56.105^\circ\text{W}$ ) and profile measurements of temperature, humidity and pressure performed by the HALO aircraft HALO, the temperature and pressure profiles are adjusted to represent the atmospheric conditions on 19 September 2014 (AC13) in the region of one of the measurement flights (representative of the three flights considered in this study). The density of water vapor is re-calculated using the relative humidity, temperature and pressure measurements. Since Rayleigh scattering is calculated from the density profile according to Bodhaine et al. (1999), the LOWTRAN (Low Resolution Transmission Model) parametrization by Pierluissi and Peng (1985), as adapted from SBDART (Santa Barbara DISORT Atmospheric Radiative Transfer) (Ricchiazzi and Gautier, 1998) is used for gas absorption. The optical properties of clouds are derived from profiles of effective radius ( $r_{\text{eff}}$ ) and liquid (ice) water content contents (LWC, IWC) using Mie calculations for water clouds, while for ice clouds the parameterizations by Baum et al. (2005, 2007) were are used. For the polluted aerosol case, aerosol properties were are described with the model by Shettle (1989) and adjusted scaled by AERONET (AEROSOL ROBOTIC NETWORK) measurements (site Alta Floresta) of aerosol optical depth, single scattering albedo, and asymmetry parameter (used for the Henyey-Greenstein phase function).

### 3 Methodology

5 The retrieval method of the phase state consists of three main steps: (3.1) The cloud masking procedure to filter illuminated cloud regions, (3.2) the cloud phase discrimination, and (3.3) the geometric allocation of the classified cloud profiles with respect to height and temperature.

#### 3.1 Cloud masking procedure

10 Compared to illuminated cloud sides, the photon paths in shadowed cloud regions are longer, which is related to more absorption events. This absorption due to cloud particles is not locally restricted to the cloud side parts where the camera is pointed at. In fact, the spectral radiation coming from shadowed cloud regions is affected by absorption by cloud particles from cloud parts outside the FOV of each individual spatial camera pixel. Since the spectral signature of reflected radiation from shadowed regions of cloud sides is contaminated by a significant fraction of diffuse radiation originating from unknown cloud regions, a cloud masking technique was developed to discriminate illuminated and shadowed cloud regions. In ground-based  
15 observations the reflected radiation measured from shadowed cloud regions showed spectral signatures influenced by the spectral surface albedo due to interaction between clouds and the surface (Jäkel et al., 2013). ~~However, for airborne measurements such spectral indication~~ This interaction is reduced for several reasons for aircraft observation of DCC. The reflected radiation is observed from higher altitudes than from the ground. This is related to changes of the range of scattering angles. Furthermore, the distances between surface and in particular the upper parts of the clouds are much larger. Therefore, scattered radiation  
20 from the immediately adjacent cloud regions has a greater effect on the spectral features in the shadowed cloud areas than the surface. Since spectral indication of the surface could neither be observed nor simulated ~~because of a different viewing geometry. Therefore for airborne measurements,~~ a different approach ~~was~~ is chosen based on the distribution of color values in the observed cloud scene. Three wavelengths ( $\lambda_B = 436$  nm,  $\lambda_G = 555$  nm, and  $\lambda_R = 700$  nm) corresponding to wavelengths of the RGB (Red Green Blue) color space are selected to calculate a simplified RGB color value for each measured spec-  
25 trum, which takes into account the sensitivity of the human eye on the different colors by differential weighting of the three wavelengths (IEC, 1999):

$$\text{RGB} = 0.2126 \cdot R + 0.7152 \cdot G + 0.0722 \cdot B \quad (1)$$

where R, G, and B represent the normalized spectral radiances. ~~In a next step the~~ The histogram of the RGB ~~values for the observed color values for each~~ cloud scene is ~~evaluated with respect to distinctive modes in the frequency distribution, indicating illuminating used to identify the illuminated~~ and shadowed cloud areas. ~~The~~  
30 Before showing an application, the procedure is illustrated using simulated cloud side reflectivity observations ~~for a cloud field that~~. In this manner, we can directly compare the classification of illuminated and shadowed cloud regions (i) derived from known cloud and viewing geometry, and (ii) derived from the histogram of the RGB color values. The cloud field was generated by the Goddard Cumulus Ensemble model (Tao et al., 2003; Zinner et al., 2008) for a model domain of  $64 \times 64$  km with a horizontal resolution of 250 m ~~and a vertical resolution between 0 and 10 km altitude of 200 m. From 10 to 120 km altitude~~

the simulations are performed with a vertical resolution ranging between 1 and 5 km. The maximum extension of the liquid water clouds from bottom to cloud top ranges from 1.0 to 7.4 km altitude. As MCARATS is a forward-propagating radiative transfer model (RTM) the simulations were performed for each grid point representing an observation altitude of 4 km.

5 The sensor is pointed at an elevation angle of  $10^\circ$  and with a relative azimuth angle to the sun of  $60^\circ$  to trigger also areas of shadowed clouds. Fig. 3a displays the RGB color values derived from the radiance simulations at each of the  $256 \times 256$  grid points. From information of the viewing geometry of the sensor and Sun (solar zenith angle  $\theta_0 = 30^\circ$ ) and the setup of the clouds in the model domain, each observed cloud pixel was classified as shadowed or illuminated. The histogram of the simulated RGB color values for all cloud observations is shown in Fig. 3b as black line. Two modes are visible, which coincide with the two sub-classes of illuminated and shadowed cloud regions (red) and shadowed (blue) cloud regions which were calculated from the cloud and viewing geometry. To identify the illuminated cloud areas for an unknown cloud geometry, as is the case for real measurements, only the brightest pixels that correspond to the right-most mode in the RGB-histogram are selected. Since the left side of this mode may also include data from shadowed regions, data larger than the maximum of this mode will be classified as illuminated and used for the cloud phase retrieval. Fig. 3e illustrates the RGB histogram for a cloud scene measured

15

The procedure is applied for an example cloud scene observed during ACRIDICON-CHUVA from 19 September 2014. During the roughly one minute flight leg the aircraft did not change its flight attitude, resulting in almost constant relative azimuth angle (angle between the sun and the viewing direction of specMACS) of  $68^\circ$  with and solar zenith angle ( $\theta_0 = 39^\circ$ ). Note, that all other selected cloud cases in this study have similar restrictions concerning the flight attitude and time period (about one minute) to guarantee comparable illumination conditions in one cloud scene. Fig. 3c illustrates the RGB histogram as calculated for observations of specMACS with an elevation ranging between  $-13$  and  $+12^\circ$ . The inlay in Fig. 3c shows the cloud situation as observed from specMACS. Applying the threshold criteria to identify the illuminated cloud parts gives a cloud mask as presented in Fig. 3d, where the illuminated cloud parts are highlighted.

20

### 25 3.2 Cloud phase discrimination

Vertical profiles of the relationship between temperature and particle size to identify the mixed phase cloud layer have been used by e.g., Rosenfeld and Woodley (2003). For continental conditions (as often observed in the Amazon Basin) the droplet size may not significantly increase between the main coalescence and mixed phase regions. Therefore, for these cases it is difficult to define the height or temperature where phase transition takes place by the increase of the droplet size. As presented in Ehrlich et al. (2008) and Jäkel et al. (2013), Jäkel et al. (2013), and Jäkel et al. (2016), another method based on differences of the refractive index of ice and liquid water between 1550 and 1700 nm wavelength can be applied to discriminate the thermodynamic water phase. The so-called phase index  $I_P$  based on spectral radiances ( $I$ ) was introduced as:

30

$$I_P = \frac{I_{1700} - I_{1550}}{I_{1700}} \quad (2)$$

~~A change of the~~ For ground-based application with corresponding viewing geometry vertical profiles of the phase index were simulated by Jäkel et al. (2013). A significant gradient in the vertical profile of the phase index was observed ~~in simulated cloud side observations~~ between liquid water and mixed phase ~~, and mixed phase layer~~, but also between mixed phase layer and ice phase, ~~respectively. Similar simulations as in Jäkel et al. (2013) using MCARATS were performed for atmospheric~~. A similar

5 ~~behavior was also found for the reflectance ratio at 2.10 and 2.25  $\mu\text{m}$  as reported by Martins et al. (2011). They observed a strong gradient in the profile of the reflectance ratio. This is due to the fact, that the imaginary part of the refractive index, which determines the spectral absorption, is different between ice and liquid water particles in the two wavelength ranges used by Martins et al. (2011) and Jäkel et al. (2013).~~

In the following, results from radiative transfer simulations using MCARATS are presented. The viewing geometry and the

10 ~~atmospheric description are adapted to the~~ conditions during ACRIDICON-CHUVA on 19 September 2014. ~~These simulations are performed to demonstrate that ice and liquid water phase can be separated from the transition layer under different conditions similar to the results reported by Jäkel et al. (2013). Note, that due to the different viewing geometry, another angular range of the scattering phase function was observed than for ground-based measurements. This might have an effect on the characteristics of phase index profile in particular with respect to separation of the mixed phase layer.~~ The model domain

15 ~~has used for the simulations had~~ 140 ~~x~~ 40 ~~x~~ 99 grid cells ~~with at~~ a horizontal resolution of 250 m and a vertical resolution of 200 m below 14 km altitude and variable resolution above. For each grid cell in a flight altitude of 8 km the spectral radiance at 1550 and 1700 nm wavelength is simulated for sensor viewing elevation angles between  $-20^\circ$  and  $+20^\circ$  corresponding to the FOV of specMACS. ~~The simulations are performed for two artificial clouds ranging between~~ Two simplified cloud scenarios

20 ~~with different profiles of cloud effective radius and water content are assumed. In both scenarios the clouds ranges from 4.0 and to~~ 11.0 km altitude with a mixed phase layer between 6.4 and 7.0 km. ~~For the first cloud case, particles with constant~~ While the first scenario uses constant values of cloud effective radius ( $r_{\text{eff}} = 20 \mu\text{m}$  for liquid water and ice ~~and constant water content of~~) and water content ( $0.7 \text{ gm}^{-3}$  ~~are assumed. For each horizontal cloud~~), the second scenario assumes variable profiles of the microphysical parameters. These two scenarios are chosen to identify effects on the  $I_P$ -profile caused by changes of (i) the phase state itself (scenario 1), and (ii) the cloud particle size and water content (scenario 2). From the 3D simulations of the

25 ~~spectral radiance at 1550 and 1700 nm the phase index is calculated following Eq. (2). For each modeled grid cell in the model domain with a horizontal~~ distance between 3 and 8 km ~~, a profile of the phase index was determined in 250 m steps. The to the cloud, a combined  $I_P$ -profile is derived from the different viewing elevation angles. Such  $I_P$ -profiles are plotted in Fig. 4a in black dots. Due to the variation of cloud distance and viewing elevation angle, the  $I_P$ -profile comprises reflected radiances originated~~ originating from various scattering angles. ~~Three~~ For the first scenario with constant microphysical parameters,

30 ~~three~~ distinct clusters corresponding to the ~~three phase states of water~~ phase state of water and the zone of phase transition, with negative values for pure liquid water, can be found. ~~The phase index is significantly shifted to positive values with some variability for~~ In the mixed phase layer ~~. The the phase index shows a steep increase to values larger than 0.15. The absolute difference of the phase index between mixed and ice phase indices between mixed phase layer and pure ice phase layer is less pronounced than between liquid and mixed phase~~. Obviously the layer. This might be caused by the fact that the contribution

35 ~~of ice particles within the mixed phase layer leads to a pronounced absorption an increased absorption of radiation~~ resulting

in an increase of the phase index. The variability of the phase index for constant microphysical conditions in each of the ~~three~~ phases is caused by the effect of the different viewing geometries. ~~Each cloud height~~ The vertical cloud structure is observed from different sensor elevation angles and distances. As the scattering phase function depends on the scattering angle, the wavelength and the particle shape, the viewing geometry of the sensor ~~related~~ relative to the position of the ~~sun~~ Sun (here:  $\theta_0 = 30^\circ$ ) also modulate the phase index. ~~Therefore, a direct conclusion on the particle size with a priori knowledge of the phase state can only be drawn when also the geometry of the observed cloud is known. For more realistic~~ The second cloud scenario assumes variable cloud microphysical properties. In general, in convective clouds, the size of ice particles is ~~larger~~ higher than the size of liquid ~~partieles, which is taken into account in the second case with variable cloud microphysical properties~~ water particles. Therefore, the second scenario represents a more realistic vertical distribution of the particle effective radius and water content than the first scenario. The corresponding vertical ~~profile~~ profiles of the effective radius and the water content of the cloud ~~is~~ are plotted in Fig. 4b. The mixed phase layer is characterized by the maximum particle sizes of liquid and ice particles over the entire profile, but lower water content compared to regions above and below. As concluded ~~in~~ by Jäkel et al. (2013), the phase index ~~gets~~ becomes less variable for a water content of more than  $0.4 \text{ g m}^{-3}$  (variation lower than 7 %) ~~which is away from the edges of DCCs. This holds true for most of the DCCs when cloud edges are excluded, which~~ are optically thinner than the inner regions of the cloud. Consequently, mainly the particle size and the phase state drive the changes of the phase index with height. Less impact is ~~attributable~~ attributed to the change of the sensor elevation angle, ~~as can be concluded from the comparison between the two cloud cases. The~~ since the variability of the phase index with respect to the viewing geometry for each phase state in the first cloud ~~case~~ scenario with fixed cloud microphysics is lower than the variability of  $I_P$  due to the changed cloud properties in the second cloud ~~case. In particular, the~~ scenario. The mixed phase layer for the second ~~case~~ scenario is characterized by a significant increase of the phase index with height. Once the pure ice phase is reached, the slope of  $I_P$  decreases. In the following, the magnitude of vertical change of the phase index will serve as indicator of the position of the mixed phase layer.

### 3.3 Cloud geometry retrieval

Due to the spatial dimension of the specMACS-SWIR instrument, reflected radiances are measured for 320 different angles with an average pixel-to-pixel spacing of about  $0.11^\circ$ . To quantify the vertical position of the mixed phase layer in terms of height or temperature, information on the cloud distance ~~needs to be gathered by independent measurements~~ is required. For that purpose, collocated images of the GoPro camera are combined with flight attitude data to apply stereo-photogrammetric methods. The theoretical background on ~~this method~~ photogrammetry is given in Hartley and Zisserman (2004), while ~~exemplarily~~ Hu et al. (2009) applied these techniques for cloud geometrical reconstruction. Basically, to The mathematics for the geometry retrieval, as it is used in this study, is based mainly on the method described by Biter et al. (1983). They deployed a side-looking camera onboard of an aircraft to detect the position of cloud features, similar to the setup presented in this work. To estimate the distance to the observed cloud element (C) two images from different positions (P1 and P2) ~~showing with~~ a projection of the observed point in both images ~~need to be taken~~ (C1 and C2, so-called tie points) ~~need to be taken (see as illustrated in Fig. 5a).~~ The point C and the two camera centers P1 and P2 define the epipolar plane. The images C1 and C2 of

5 ~~C in the two images lie on this plane. In fact, the~~. The geometric problem comprises three ~~different coordinate systems, one~~ coordinate systems: for the camera, ~~one for~~ the aircraft, and the world coordinate system (longitude, latitude and altitude) for the observed point C. ~~Therefore, coordinate~~ (Biter et al., 1983). Coordinate transformations are required to relate the different coordinate systems. Fig. 5b illustrates the aircraft and camera coordinate system, which differ because the GoPro camera looks perpendicular to the flight direction. ~~Exemplarily~~ For example, a positive pitch angle of the aircraft (associated with rotation around the aircraft  $y_a$ -axis) rotates the camera (image) around the camera's  ~~$x$ -axis~~. ~~The  $x_i$ -axis as can be deduced from Fig.~~ 5b. The  $x$ - and  $y$ -axis- $y$ -axis of the world coordinate system (not shown) are pointed to the east and to the north, respectively, while the  ~~$z$ -axis~~  $z$ -axis is perpendicular to the  ~~$x$ - $y$~~   $x$ - $y$  plane (pointing upward). Each selected image in the camera system ( ~~$x_i, y_i, z_i$~~   $x_i, y_i, z_i$ ) is transformed into the aircraft coordinate system ( ~~$x_a, y_a, z_a$~~   $x_a, y_a, z_a$ ), and finally into the world system ( ~~$x_w, y_w, z_w$~~   $x_w, y_w, z_w$ ). This transformation requires the rotation of the coordinate systems with respect to the three Euler angles pitch, roll, and yaw using the 3  ~~$\times$~~   $\times$  3 rotation matrices for the aircraft to world [ $\mathbf{R}_w^a$ ], and camera to aircraft [ $\mathbf{R}_a^i$ ] system:

$$\begin{bmatrix} x_w \\ y_w \\ z_w \end{bmatrix} = [\mathbf{R}_w^a][\mathbf{R}_a^i] \begin{bmatrix} x_i \\ y_i \\ z_i \end{bmatrix} \quad (3)$$

The general form of the two rotation matrices for system 1 to system 2 (either "a" to "w" or "i" to "a") are:

$$[\mathbf{R}_2^1] = \begin{bmatrix} \cos \psi \cos \theta & \cos \psi \sin \theta \sin \phi + \sin \psi \cos \phi & -\cos \psi \sin \theta \cos \phi + \sin \psi \sin \phi \\ -\sin \psi \cos \theta & -\sin \psi \sin \theta \sin \phi + \cos \psi \cos \phi & \sin \psi \sin \theta \cos \phi + \cos \psi \sin \phi \\ \sin \theta & \cos \theta \sin \phi & \cos \theta \cos \phi \end{bmatrix} \quad (4)$$

with  $\phi = -(\phi_a - 180^\circ)$ ,  $\theta = \theta_a$ , and  $\psi = (\psi_a - 90^\circ)$  for aircraft to world coordinates and  $\phi = -\phi_i$ ,  $\theta = -\theta_i$ , and  $\psi = -\psi_i$  for camera to aircraft coordinates.

After coordinate transformation, trigonometric methods (Biter et al., 1983) are applied to calculate the distance between the camera positions P1 and P2 to the observed point C. Repeating this procedure for a number of points yields a relation between elevation angle and cloud height. Note, that the elevation angle represents the elevation angle of the selected tie point of the camera image after correction based on the aircraft attitude data. It gives the elevation angle above or below the flight altitude.

25 For better selection of the tie points, which is done manually, the contrast of the images ~~was~~ is increased for better identification of recognizable structures of the cloud image. Fig. 6 illustrates the cloud geometry retrieval for a cloud scene from 19 September 2014. The selected cloud ~~ease-scene~~ shows a strong convective cloud embedded in a stratiform cloud layer. After increasing the image contrast (Fig. 6a) several tie points with distinctive cloud features of individual clouds were selected. The same tie points ~~were~~ are chosen in a second image taken about 10 seconds later. Choosing a short time interval helps to reduce the uncertainty of the method induced by cloud movement. From stereographic analysis of these tie points the distances to the cloud points ~~were~~ (in km) are determined (Fig. 6b). From cloud distance and viewing elevation angle the height ~~was~~ is calculated. Cloud top heights for this case are in the range of 12 km, while the top of the stratiform layer is at about 6 km altitude. The corresponding isolines in Fig. 6c show quite a homogeneous horizontal distribution with negligible dependence on the azimuth angle for this

5 particular cloud case. Therefore, the correlation between elevation angle and height ~~was~~ is approximated by a polynomial fit of

the third order as plotted in Fig. 6d. This fit ~~was~~is used to relate the elevation angles of the specMACS instrument to a cloud height. For all studied cloud cases of the flights AC10, AC13, and AC18, such simplified correlations between elevation angle and height ~~were~~are determined under the condition that the azimuthal dependence could be neglected which ~~was~~is fulfilled predominantly for sufficiently small cloud sections in the horizontal direction.

10 The accuracy of the cloud geometry retrieval depends ~~mainly~~ on the distance to the observed cloud and the uncertainty of the angle determination. Uncertainties related to pixel selection ~~were determined~~are estimated with  $\pm 5$  pixels ( $0.25^\circ$ ), which corresponds to an uncertainty of 130 m for a cloud distance of 30 km (maximum distance of observations). Additionally, the fitting method ~~resulted~~results in mean deviations of 200 m. Overall, uncertainties between 200 and 300 m ~~were~~are calculated for the observing conditions during ACRIDICON-CHUVA.

## 15 4 Application

### 4.1 ~~Case study for flight AC13 (polluted aerosol conditions)~~

~~Results of the analysis of one of the~~From the 14 scientific flights ~~during ACRIDICON-CHUVA will be presented in this section in more detail. To derive cloud profiles of the phase state based on cloud side spectral reflectivity observations several conditions need to be fulfilled~~three days (AC10, AC13, and AC18) are selected with the best observation conditions for specMACS,

20 namely: (i) no cloud layer above the observed cloud (no cirrus), which contaminates the spectral signature, (ii) high proportion of illuminated cloud parts in the vertical direction of the cloud, (iii) flight altitude that allows measurements of an extended vertical region of the cloud considering the limited FOV of specMACS, and (iv) isolated clouds with recognizable structures for cloud geometry retrievals.

Phase profiles from AC13 representing polluted aerosol conditions will be compared to the two days with less aerosol pollution.

25 Effects of aerosol conditions on the height and thickness of the mixed phase layer will be investigated. Second, it will be demonstrated how comparable the different observation strategies (cloud side, cloud top and in situ) are.

### 4.1 ~~Case study for flight AC13 (polluted aerosol conditions)~~

During flight AC13 on 19 September 2014, several periods of cloud side observations ~~were found that fulfill these conditions~~are found. The flight track and the corresponding MODIS image ~~is~~are shown in Fig. 7. The 250 m resolution radiance of channel 1

30 (620-670 nm) of the MODIS overpass from 17:50 UTC illustrates the cloud coverage. The five colored lines denote the periods of cloud side observations between 17:50 and 19:00 UTC. The white arrows indicate the flight direction with specMACS pointing towards the clouds on the right hand side of the aircraft. The flight altitude for this one-hour flight track ranged between 5 and 10 km. As a result of cloud masking and cloud geometry analysis, the profile of the phase index for a cloud scene (section #A in Fig. 7) is shown in Fig. 8. The phase index is calculated in bins of 100 m in the vertical direction. The standard deviation is indicated by the error bars. A distinctive increase of the phase index is visible at 6.5 km altitude. Below that altitude a negative phase index indicating the liquid water phase ~~was~~is derived. Within the mixed phase layer the phase

index increases sharply. The upper limit of the mixed phase layer is derived to be at 7.1 km. Above that altitude the variation of the phase index caused by changing particle sizes and viewing geometry is less pronounced.

- 5 Sixteen cloud cases ~~have been are~~ investigated for flight AC13. Each cloud scene ~~was is~~ classified with respect to the phase state based on the profile of the phase index. Fig. 9a presents the statistics over all scenes. The background color of the scene number corresponds to the flight section as presented in Fig. 7. Obviously not all profiles show each of the ~~three phase states. Mainly~~ phase states, mainly because of two reasons. First, the cloud particles may have the same phase state, or, second, the viewing geometry with respect to FOV, flight altitude, cloud height, and distance restricts the vertical range of the cloud observation.
- 10 Overall, the depth ( $\Delta z_{\text{mix}}$ ) and vertical position ( $z_{\text{top}}$ ,  ~~$z_{\text{bottom}}$~~   $z_{\text{bot}}$ ) of the mixed phase layer is highly variable for all cases: with  $\Delta z_{\text{mix}} = 1.2 \pm 0.4$  km (one-sigma standard deviation),  ~~$z_{\text{bottom}}$~~   $z_{\text{bot}} = 6.2 \pm 0.3$  km, and  $z_{\text{top}} = 7.4 \pm 0.4$  km. Even for similar flight sections (as in #B and #D) the upper and lower limit of the mixed phase layer can vary by up to 900 m, which is larger than the uncertainty of the retrieval method. The corresponding temperature scale is displayed as non-linear secondary y-axis.
- 15 ~~In situ~~ The variability of the mixed phase layer in depth and height within a single cloud cluster shows that the vertical distribution at least at the cloud edges is variable. In situ data are used to investigate if such a variability is also observed in the the more inner part of the cloud? In situ measurements of CAS-DPOL and hotwire data of the one-hour flight sequence (17:50-19:00 UTC) during AC13 are shown in Fig. 9b,c. The light dots are 1Hz data, while darker lines represent the 10th and 90th percentiles as well as the mean LWC and AF (squares), binned into 600 m altitude bins. Regions of mixed phase
- 20 clouds are characterized by a decrease in LWC (decrease of the 90th percentile with altitude) and/or an increase in AF. In these in situ measurements of LWC and AF, the mixed phase region extends between 6.4 and 8.7 km. However, the profiles shown in Fig. 9b,c are based on data sampled over the entire cloud cluster including clouds at different stages of evolution, and profiles of individual clouds cannot be derived from this data set, which prevents a direct comparison of the in situ and remote measurements. The asphericity of cloud particles in the size range 20 - 50  $\mu\text{m}$  derived from NIXE-CAPS is shown in Fig. 9d for
- 25 the one hour time frame of the cloud observations. The data ~~were are~~ classified as listed in Tab. 2. The heterogeneity of cloud particle asphericity between 5 and 8 km altitude ~~can be is~~ observed from its variable classification during the ascent around 18 UTC with solely spherical particles (could be also related to small spherical ice particles) and during the descent between 18.25 and 18.80 UTC with spherical and aspherical particles. Mainly aspherical particles of Group II ~~were are~~ observed, indicating the existence of large ice particles with sizes larger than 50  $\mu\text{m}$ . Except for two single cases, a larger number of spherical
- 30 particles (open green circles) ~~can be is~~ observed up to an altitude of 8 km. From the descent flight track the position of the mixed phase layer is estimated between 6 and 8 km. ~~Exemplarily~~ For example, a closer look at the asphericity is taken for the time range between 18.28 and 18.34 UTC (Fig. 9e). At a constant flight level near the upper boundary of the mixed phase layer the occurrence of spherical and aspherical particles is somewhat separated. While mainly spherical particles ~~were are~~ observed during this selected flight section for vertical wind speeds between  $\pm 1 \text{ m s}^{-1}$ , there are also segments with higher
- 35 vertical wind speeds (between -3 and 5  $\text{m s}^{-1}$ ). For this section (around 18.315 UTC) large aspherical particles representing ice particles were also measured. This suggests that the vertical distribution of ice and liquid particles is affected by up- and downdrafts within a convective cloud, and therefore it is not homogenous inside the same cloud.

After showing these results from in situ and cloud side measurements, we also present retrievals of the phase state based on cloud top MODIS observations. In Fig. 9f the frequency of liquid and ice phase observations for altitude bins of about 200 m is presented. ~~In these retrievals, no mixed phase was derived for all data in the selected area (Fig. 7). Either fully~~ Fully developed deep convective clouds with cloud tops between 10 and 14 km (classified as ice cloud) ~~or and~~ low level cumulus clouds up to 6 km (liquid water clouds) ~~were are~~ detected. Cloud phase information from the assumed ~~mixed phase levels are not available~~ ~~, since no cloud tops with mixed phase were observed.~~ ~~phase transition layers is not available in Collection 6.~~ Nevertheless, there are some levels with low frequency classified as ice and liquid phase (8 - 11 km), corresponding to temperatures between 10 -20 and -42°C. In particular, at very low temperatures (lower than -38 °C) the presence of liquid particles can be excluded even for situations of homogeneous freezing. In fact small ice particles may be misinterpreted as liquid particles by the retrieval algorithm at this level (Järvinen et al., 2016).

We applied the ensemble method to derive profiles of the effective particle size and to estimate the glaciation height and temperature following the retrieval technique of Yuan et al. (2010) for the MODIS scene. For better comparison, the brightness 15 temperature as vertical coordinate ~~was is~~ converted to altitude. Cloud top brightness temperatures (at 11 μm, corresponding to MODIS Channel 31) ~~were are~~ simulated for variable cloud top heights and an atmospheric profile of temperature and humidity as measured by the aircraft. The best agreement of simulated and measured cloud top brightness temperature is used as proxy of the cloud top altitude. The result is presented in Fig. 9g. The particle size is increasing with altitude up to a height of about 9.0 km (horizontal black line). This level is assumed as glaciation height, the upper level of mixed phase layer. The standard 20 deviation of the binned (2 K bins in brightness temperature) particle sizes (horizontal error bars) is significantly larger for altitudes below 11 km, indicating a larger variability of the cloud particle size and a smaller statistics. ~~Furthermore, a second but smaller peak of the particle size is found at about 6 km altitude. From the conceptual model of cloud particle size profiles inside a DCC (e.g., Rosenfeld and Woodley (2003)) it might indicate the bottom of the mixed phase layer, when cloud particle size starts to increase. However, this increase is less pronounced than presented in Rosenfeld and Woodley (2003).~~

25 Comparing the glaciation height from MODIS with NIXE-CAPS in situ data and results from specMACS observations shows a deviation of about 1.0 - 1.5 km between the different retrieval techniques and observation strategies. However, the mean profile over the entire cloud cluster derived from CAS-DPOL measurements exhibited a similar glaciation height (of about 8.7 km) as found from the MODIS data. This shows that the satellite-based ensemble method may be representative for a large cloud field; ~~but that.~~ ~~But~~ for individual clouds ~~, particularly in their later stage of evolution~~ ~~NIXE-CAPS and specMACS measurements~~ 30 ~~have shown lower glaciation heights. The most likely reason is related to the fact that the ensemble method relies on cloud top observations of growing clouds in different stages of evolution. As shown in Fig. 9g mainly particle sizes between 22 and 27 μm are derived indicating that the profile is dominated by measurements of clouds in the mature stage. At this stage,~~ the particle phase may be altered by up- and downdrafts ~~as observed by the NIXE-CAPS and specMACS measurements~~ ~~within the clouds~~ as was shown in Fig. 9e. This leads to an enhanced horizontal variability of the cloud phase state which cannot be resolved by passive remote sensing from cloud top observations. Another, but minor reason of the discrepancy between ensemble method and NIXE-CAPS / specMACS measurements is related to the retrieval uncertainty of the effective cloud particle radius. While scattering properties are well defined for liquid water particles, they are variable for ice particles due to differing habits and

crystal shapes (Eichler et al., 2009). This gets even more complicated for cloud tops where phase transition starts. Additional retrieval uncertainties of the particle size directly contribute to the derived profile of  $r_{\text{eff}}$ .

## 4.2 Comparison with less polluted conditions

Profiles of the phase state for two other flights (AC10 and AC18) performed under moderate aerosol conditions are presented in Fig.10. On both days the number of complete profiles showing ~~all three phases is limited~~ liquid, ice and the mixed phase layer is smaller compared to AC13. Mainly low level clouds or cloud parts with liquid water were observed ~~on~~ during AC18. The lower boundary of the mixed phase layer is estimated to be about 5.5 km ( $-4^{\circ}\text{C}$ ). From NIXE-CAPS measurements, large aspherical ice particles ~~were measured~~ are found down to 5 km ( $-1^{\circ}\text{C}$ ), whereas spherical particles assumed to be as liquid water were ~~found~~ observed up to 8.7 km (~~not shown~~). In contrast, the specMACS data exhibit ice phase down to 7.7 km. As in the case of AC13, the cloud top MODIS retrievals of the phase state only ~~distinguished~~ distinguishes between liquid and ice phase. Because of the low statistical significance of clouds with cloud tops higher than 6 km in the MODIS data, no profile of effective drop radius ~~was derived. From theory the mixed phase layer is expected to be higher for polluted aerosol conditions than for cleaner aerosol conditions, which could not be confirmed by the studied cases. It was evident, however, that the lower boundary altitude of the mixed phase layer tends to be higher for polluted conditions (AC13: 6.0–6.5 km) than for the moderate case of AC18. is derived.~~

On flight AC10 no in situ data within mixed phase clouds ~~was obtained. Also the~~ were obtained. The MODIS phase product shows ~~either ice (ice cloud tops between 11 and 15 km altitude ) or liquid water (and liquid water clouds up to 4.5 km)~~. But the profile of the effective particle radius based on the ensemble method retrieval gives a glaciation temperature of 260 K, which corresponds to an altitude of about 7.2 km. The specMACS profiles as plotted in Fig. 10b show highly variable mixed phase layers. While clouds #1 - #3 with cloud tops between 6.0 - 6.8 km ~~were~~ are classified as liquid water clouds, the ~~profile~~ profiles of the phase index of clouds #4 - #6 reveal also the existence of ice particles between 4 and 7 km altitude. As illustrated in the RGB image taken by the GoPro camera (Fig. 10c), cloud #3 and #4 ~~were~~ are in close vicinity but in different states of evolution. The diffuse ~~looking~~ cloud areas with smoother texture in the GoPro image of cloud #4 indicate precipitation, which explains positive phase indices down to 4 km corresponding to ~~more than~~  $0^{\circ}\text{C}$ . As Fig. 10d ~~clearly~~ shows, the phase index can vary significantly for one altitude level depending on the occurrence of precipitation. Consequently, the individual state of evolution of each cloud determines the distribution of particle sizes and phase state. Also ~~local~~ strong downdrafts can transport ice particles into lower levels, which will be interpreted as mixed phase layer from the cloud side observation perspective; ~~whereas~~. ~~Due to the horizontal variability of cloud phase inside a cloud cluster for example caused by up- and downdrafts,~~ in situ measurements ~~inside the cloud may~~ only reveal liquid phase particles. ~~A direct comparison between the observation strategies is subject to restrictions because of temporal and spatial variability of cloud properties in convective systems.~~ ~~From theory, the mixed phase layer is expected to be higher for polluted aerosol conditions than for cleaner aerosol conditions, which can partly be confirmed by comparison of the three cases. We find from cloud side observations, that the lower boundary altitude of the mixed phase layer tends to be higher for polluted conditions (AC13: 6.0 - 6.5 km) than for the moderate case of~~

AC18 ( $5.6 \pm 0.2$  km), while the upper boundary is shifted from  $6.8 \pm 0.2$  km (moderate case AC10) to  $7.4 \pm 0.4$  km (polluted case AC13).

## 5 5 Conclusions

The vertical evolution of deep convective clouds is linked with the phase transition from liquid water ~~to mixed phase and to the ice phase via the mixed phase to ice~~. Aerosol particles may alter the radiative effects of cloud particles (also with respect to their phase state), their lifetime and the formation of precipitation. This study ~~documents~~ documented the vertical distribution of the ~~three phase states cloud phase~~ for different aerosol conditions as measured during the ACRIDICON-CHUVA campaign over the Brazilian Amazon rainforest in September 2014. ~~A different approach than the traditional in situ and satellite observations was presented, which is mainly focused on the retrieval~~ Our approach applies a retrieval method to quantify the height range of the mixed phase layer. Cloud side observations performed by ~~the imaging spectroradiometer speeMACS an imaging spectroradiometer~~ were used to determine a phase index based on differential absorption by ice and liquid water in the spectral range between 1550 and 1700 nm. Negative values of the phase index indicate liquid particles, whereas ice particles ~~cause are characterized by~~ a positive phase index. It was ~~additionally~~ shown by 3D radiative transfer simulations that the mixed phase zone is characterized by a ~~distinctive change of significant~~ gradient in the profile of the phase index. A cloud mask method to discriminate between shadowed and illuminated cloud regions was presented to exclude the shadowed areas in the cloud scene ~~due to their contaminated spectral information. We also performed~~. 3D radiative transfer simulations ~~for a complex cloud field were performed~~ to validate the approach ~~of using histograms of RGB color values for the discrimination method. Since speeMACS~~. Since the imaging spectroradiometer delivers spectral radiation data as a function of viewing zenith angle, the derived mean vertical profiles of the phase index needed to be referenced to altitude ranges. For this purpose, stereographic methods were applied to collocated GoPro camera observations to estimate the cloud geometry in terms of cloud height profiles and distance to the aircraft.

The profiles of several individual clouds were classified with respect to their zones of phase states. Depending on the viewing geometry and cloud distance, ~~all three phases were found for deep convective clouds. In particular the layer of phase transition was highly~~ layers of pure liquid and ice phase, as well as phase transition layers were identified. It was found that the height and thickness of the layers of phase transition were variable (900 m in upper and lower limit) ~~in its height and vertical thickness~~ even for one compact cloud cluster measured during flight AC13 with polluted aerosol conditions. Here first ice particles were found at temperatures between  $-3$  and  $-9$  °C, while full glaciation was observed between  $-10$  and  $-20$  °C. ~~Only few cases showing all three phase states were observed for~~ For moderate aerosol conditions. ~~Because of the low statistics,~~ only few cases exhibited liquid water, mixed phase, and ice phase, which limited the statistical significance of the comparison with AC13. However, comparing the glaciation heights of AC10 ( $6.8 \pm 0.2$  km) and AC13 ( $7.4 \pm 0.4$  km) we found an indication of an increase of glaciation height and a decrease of glaciation temperature for polluted aerosol conditions ~~compared to the moderate case of flight AC18 could not be observed. However, the~~. With respect to the occurrence of first ice particles ~~was found for polluted conditions between~~, the lower boundary of the mixed phase layer was derived with  $6.0 - 6.5$  km for polluted conditions, whereas for AC18 the altitude was shifted down to  $5.5 - 6.0$  km, which agrees with theory.

Also, in situ measurements of the cloud particle size distribution together with the asphericity of particles between  $20$  and  $50$   $\mu\text{m}$ , measured by the cloud spectrometer NIXE-CAPS, were used to estimate the cloud's phase (Costa et al., 2017). Aspher-

ical ~~hydrometeor~~ particles can be considered as ice, whereas spherical shapes are related to liquid droplets or spherical ice. In contrast to cloud-side remote sensing ~~by specMACS~~, in situ observations represent point measurements within the cloud. Therefore, in situ profile information of an individual cloud is a combination of data from different ~~time-steps and therefore~~ states of evolution. ~~Despite the different observation perspectives, consistent results were found with similar mixed phase zone~~

5 ~~levels~~ Consistent results of mixed phase zone levels were found from specMACS and NIXE-CAPS measurements, for the flight AC13 with most individual cloud cases showing pure liquid, mixed phase layer and pure ice phase.

~~Aerosol effects on~~ Additionally to in situ and cloud side measurements, the glaciation temperature ~~in deep convective clouds were studied with~~ was derived applying an ensemble method ~~using based on~~ MODIS data, which assumes ~~the invariance of space and time~~ time-space-exchangeability for a cluster of clouds with different states of evolution. For the polluted and moderate flights, retrieval results of the effective particle size at cloud top were combined into one single profile. For flight AC13 the glaciation height of 9.0 km (-26°C), defined by the level of maximum particle size, deviates from the in situ (8 km) and specMACS results (6.8 - 8.2 km). However, for the moderate aerosol case the glaciation height ~~is was~~ much lower at about 7.2 km (-13°C), similar to the height derived from specMACS observations (7 km).

The presented study ~~shows has shown~~ that the occurrence of ice particles and the level of the mixed phase layer vary by several hundred of meters even for similar atmospheric conditions. Two cloud cases in close vicinity clearly show different cloud phases at the same altitude. It is assumed that downdrafts and falling precipitation in well-developed clouds alter the retrieval results of the phases' vertical distribution. ~~Finally, we can conclude~~ It is concluded that the assumed ~~space-time-invariance~~ time-space-exchangeability used in the ensemble method can give ~~only~~ a simplified picture of the vertical distribution of the phase within a field of convective clouds of different stages of evolution. Particularly, cloud tops where phase transition

20 (from liquid to ice) starts and ends needs to be observed by the satellite to profile the thermodynamic phase. The number of these observations has to be significant, since the particle sizes are averaged over a larger domain. So, in general the ensemble method can give an indication when phase transition arises for the first time. However, for estimation of the cloud phase profile at a later stage of the DCC evolution, in situ and also cloud side remote sensing might be the better observation strategy, when phase distribution is altered for example by up- and downdrafts.

Planned future studies include observations of individual convective clouds to document their evolution from growing to mature and finally to dissipating stages of development. We intend to deploy our sensor on ATTO (Andreae et al., 2015), which

5 is 325 m high and is used to perform continuous monitoring of chemical, meteorological and aerosol parameters. The ATTO tower is located near the Equator (a region with daily occurrence of DCCs in a highly variable environment with respect to concentrations and types of aerosol particles) and will serve as an ideal platform for upcoming studies.

*Acknowledgements.* The ACRIDICON-CHUVA campaign was supported by the Max Planck Society (MPG), the German Science Foundation (DFG Priority Program SPP 1294), the German Aerospace Center (DLR), the FAPESP (Sao Paulo Research Foundation) grants

10 2009/15235-8 and 2013/05014-0), and a wide range of other institutional partners. It was carried out in collaboration with the USA-Brazilian atmosphere research project GoAmazon2014/5, including numerous institutional partners. We would like to thank Instituto Nacional de Pesquisas da Amazonia (INPA) for the local logistic help prior, during, and after the campaign. Thanks also to the Brazilian Space Agency (AEB: Agencia Espacial Brasileira) responsible for the program of cooperation (CNPq license 00254/2013-9 of the Brazilian National Council for Scientific and Technological Development). The entire ACRIDICON-CHUVA project team is gratefully acknowledged for col-

15 laboration and support. Evelyn Jäkel gratefully acknowledges funding of parts of this work by the German Research Foundation (DFG) under grant number (JA2023/2-2).

## References

- Albrecht, B. A.: Aerosols, cloud microphysics, and fractional cloudiness, *Science*, 245, 1227–1230, <http://www.sciencemag.org/content/245/4923/1227.abstract>, 1989.
- 20 Anderson, G., Clough, S., Kneizys, F., Chetwynd, J., and Shettle, E.: AFGL Atmospheric Constituent Profiles (0–120 km), Tech. Rep. AFGL-TR-86-0110, AFGL (OPI), Hanscom AFB, MA 01736, 1986.
- Andreae, M. O., Rosenfeld, D., Artaxo, P., Costa, A. A., Frank, G. P., Longo, K. M., and Silva-Dias, M. A. F.: Smoking rain clouds over the Amazon, *Science*, 303, 1337–1342, doi:10.1126/science.1092779, 2004.
- Andreae, M. O., Acevedo, O. C., Araùjo, A., Artaxo, P., Barbosa, C. G. G., Barbosa, H. M. J., Brito, J., Carbone, S., Chi, X., Cintra, B.,  
25 B. L., da Silva, N. F., Dias, N. L., Dias-Júnior, C. Q., Ditas, F., Ditz, R., Godoi, A. F. L., Godoi, R. H. M., Heimann, M., Hoffmann, T., Kesselmeier, J., Könemann, T., Krüger, M. L., Lavric, J. V., Manzi, A. O., Lopes, A. P., Martins, D. L., Mikhailov, E. F., Moran-Zuloaga, D., Nelson, B. W., Nölscher, A. C., Santos Nogueira, D., Piedade, M. T. F., Pöhlker, C., Pöschl, U., Quesada, C. A., Rizzo, L. V., Ro, C.-U., Ruckteschler, N., Sá, L. D. A., de Oliveira Sá, M., Sales, C. B., dos Santos, R. M. N., Saturno, J., Schöngart, J., Sörgel, M., de Souza, C. M., de Souza, R. A. F., Su, H., Targhetta, N., Tóta, J., Trebs, I., Trumbore, S., van Eijck, A., Walter, D., Wang, Z.,  
30 Weber, B., Williams, J., Winderlich, J., Wittmann, F., Wolff, S., and Yáñez Serrano, A. M.: The Amazon Tall Tower Observatory (ATTO): overview of pilot measurements on ecosystem ecology, meteorology, trace gases, and aerosols, *Atmos. Chem. Phys.*, 15, 10723–10776, doi:10.5194/acp-15-10723-2015, <http://www.atmos-chem-phys.net/15/10723/2015/>, 2015.
- Baum, B. A., Heymsfield, A. J., Yang, P., and Bedka, S. T.: Bulk scattering properties for the remote sensing of ice clouds. Part I: Microphysical data and models, *J. Appl. Meteor.*, 44, 1885–1895, 2005.
- 35 Baum, B. A., Yang, P., Nasiri, S., Heidinger, A. K., Heymsfield, A., and Li, J.: Bulk scattering properties for the remote sensing of ice clouds. Part III: High-resolution spectral models from 100 to 3250  $\text{cm}^{-1}$ , *J. Appl. Meteor.*, 46, 423–434, 2007.
- Baum, B. A., Menzel, W. P., Frey, R. A., Tobin, D. C., Holz, R. E., Ackerman, S. A., Heidinger, A. K., and Yang, P.: MODIS Cloud-Top Property Refinements for Collection 6, *Journal of Applied Meteorology and Climatology*, 51, 1145–1163, doi:10.1175/JAMC-D-11-0203.1, <http://dx.doi.org/10.1175/JAMC-D-11-0203.1>, 2012.
- Biter, C. J., Cannon, T. W., Crow, E. L., Knight, C. A., and Roskowski, P. M.: Improvements in Cloud Photogrammetry Using Airborne, Side-Looking, Time-Lapse Cameras, *Journal of Climate and Applied Meteorology*, 22, 1047–1055, doi:10.1175/1520-0450(1983)022<1047:IICPUA>2.0.CO;2, [http://dx.doi.org/10.1175/1520-0450\(1983\)022<1047:IICPUA>2.0.CO;2](http://dx.doi.org/10.1175/1520-0450(1983)022<1047:IICPUA>2.0.CO;2), 1983.
- 5 Bodhaine, B., Wood, N., Dutton, E., and Slusser, J.: On Rayleigh optical depth calculations, *J. Atmos. Oceanic Technol.*, 16, 1854–1861, 1999.
- 10 Bradski, G. and Kaehler, A.: *Learning OpenCV: Computer Vision in C++ with the OpenCV Library*, O’Reilly Media, Inc., 2nd edn., 2013.
- Braga, R. C., Rosenfeld, D., Weigel, R., Jurkat, T., Andreae, M. O., Wendisch, M., Pöhlker, M. L., Klimach, T., Pöschl, U., Pöhlker, C., Voigt, C., Mahnke, C., Borrmann, S., Albrecht, R. I., Molleker, S., Vila, D. A., Machado, L. A. T., and Artaxo, P.: Comparing calculated microphysical properties of tropical convective clouds at cloud base with measurements during the ACRIDICON-CHUVA campaign, *Atmospheric Chemistry and Physics Discussions*, 2016, 1–46, doi:10.5194/acp-2016-872, <http://www.atmos-chem-phys-discuss.net/acp-2016-872/>, 2016.
- 15 Cahalan, R.: Bounded cascade clouds: albedo and effective thickness, *Nonlin. Proc. Geophys.*, 1, 1994.

- Cecchini, M. A., Machado, L. A. T., Andreae, M. O., Martin, S. T., Albrecht, R. I., Artaxo, P., Barbosa, H. M. J., Borrmann, S., Fütterer, D., Jurkat, T., Mahnke, C., Minikin, A., Molleker, S., Pöhlker, M. L., Pöschl, U., Rosenfeld, D., Voigt, C., Wenzierl, B., and Wendisch, M.: Sensitivities of Amazonian clouds to aerosols and updraft speed, *Atmospheric Chemistry and Physics Discussions*, 2017, 1–23, doi:10.5194/acp-2017-89, <http://www.atmos-chem-phys-discuss.net/acp-2017-89/>, 2017a.
- Cecchini, M. A., Machado, L. A. T., Wendisch, M., Costa, A., Krämer, M., Andreae, M. O., Afchine, A., Albrecht, R. I., Artaxo, P., Borrmann, S., Fütterer, D., Klimach, T., Mahnke, C., Martin, S. T., Minikin, A., Molleker, S., Pardo, L. H., Pöhlker, C., Pöhlker, M. L., Pöschl, U., Rosenfeld, D., and Wenzierl, B.: Illustration of microphysical processes in Amazonian deep convective clouds in the Gamma phase space: Introduction and potential applications, *Atmospheric Chemistry and Physics Discussions*, 2017, 1–49, doi:10.5194/acp-2017-185, <http://www.atmos-chem-phys-discuss.net/acp-2017-185/>, 2017b.
- Costa, A., Meyer, J., Afchine, A., Luebke, A., Günther, G., Dorsey, J. R., Gallagher, M. W., Ehrlich, A., Wendisch, M., Baumgardner, D., Wex, H., and Krämer, M.: Classification of Arctic, Mid-Latitude and Tropical Clouds in the Mixed-Phase Temperature Regime, *Atmospheric Chemistry and Physics Discussions*, 2017, 1–40, doi:10.5194/acp-2017-226, <http://www.atmos-chem-phys-discuss.net/acp-2017-226/>, 2017.
- Ehrlich, A., Bierwirth, E., Wendisch, M., Gayet, J.-F., Mioche, G., Lampert, A., and Heintzenberg, J.: Cloud phase identification of Arctic boundary-layer clouds from airborne spectral reflection measurements: Test of three approaches, *Atmos. Chem. Phys.*, 8, 7493–7505, 2008.
- Eichler, H., Ehrlich, A., Wendisch, M., Mioche, G., Gayet, J.-F., Wirth, M., Emde, C., and Minikin, A.: Influence of ice crystal shape on retrieval of cirrus optical thickness and effective radius: A case study, *J. Geophys. Res.*, 114, D19203, doi:10.1029/2009JD012215, 2009.
- Ewald, F., Winkler, C., and Zinner, T.: Reconstruction of cloud geometry using a scanning cloud radar, *Atmos. Meas. Tech.*, 8, 2491–2508, doi:10.5194/amt-8-2491-2015, 2015.
- Ewald, F., Kölling, T., Baumgartner, A., Zinner, T., and Mayer, B.: Design and characterization of specMACS, a multipurpose hyperspectral cloud and sky imager, *Atmos. Meas. Technol.*, 9, 2015–2042, doi:10.5194/amt-9-2015-2016, 2016.
- Freud, E., Rosenfeld, D., Andreae, M. O., Costa, A. A., and Artaxo, P.: Robust relations between CCN and the vertical evolution of cloud drop size distribution in deep convective clouds, *Atmos. Chem. Phys.*, 8, 1661–1675, 2008.
- Hartley, R. I. and Zisserman, A.: *Multiple View Geometry in Computer Vision*, Cambridge University Press, ISBN: 0521540518, second edn., 2004.
- Hu, J., Razdan, A., and Zehnder, J. A.: Geometric Calibration of Digital Cameras for 3D Cumulus Cloud Measurements, *J. Atmos. Oceanic Technol.*, 26, 200–214, doi:10.1175/2008JTECHA1079.1, <http://dx.doi.org/10.1175/2008JTECHA1079.1>, 2009.
- IEC: *Multimedia Systems and Equipment – Colour Measurements and Management – Part 2-1: Colour Management – Default RGB Color Space – sRGB*, IEC 61966-2-1, International Electrotechnical Commission: Geneva, Switzerland, 1999.
- Iwabuchi, H.: Efficient Monte Carlo methods for radiative transfer modeling, *J. Atmos. Sci.*, 63, 2324–2339, 2006.
- Jäkel, E., Walther, J., and Wendisch, M.: Thermodynamic phase retrieval of convective clouds: impact of sensor viewing geometry and vertical distribution of cloud properties, *Atmos. Meas. Tech.*, 6, 539–547, doi:10.5194/amt-6-539-2013, 2013.
- Jäkel, E., Wendisch, M., Ewald, F., and Kölling, T.: Analysis of the Vertical Distribution of the Thermodynamic Phase in Tropical Deep-convective Clouds, in: *Light, Energy and the Environment*, p. HTu2F.1, Optical Society of America, doi:10.1364/HISE.2016.HTu2F.1, <http://www.osapublishing.org/abstract.cfm?URI=HISE-2016-HTu2F.1>, 2016.

- Järvinen, E., Schnaiter, M., Mioche, G., Jourdan, O., Shcherbakov, V. N., Costa, A., Afchine, A., Krämer, M., Heidelberg, F., Jurkat, T., Voigt, C., Schlager, H., Nichman, L., Gallagher, M., Hirst, E., Schmitt, C., Bansemmer, A., Heymsfield, A., Lawson, P., Tricoli, U., Pfeilsticker, K., Vochezer, P., Möhler, O., and Leisner, T.: Quasi-Spherical Ice in Convective Clouds, *Journal of the Atmospheric Sciences*, 73, 3885–3910, doi:10.1175/JAS-D-15-0365.1, <http://dx.doi.org/10.1175/JAS-D-15-0365.1>, 2016.
- 20 Khain, A., Prabha, T. V., Benmoshe, N., Pandithurai, G., and Ovchinnikov, M.: The mechanism of first raindrops formation in deep convective clouds, *Journal of Geophysical Research: Atmospheres*, 118, 9123–9140, doi:10.1002/jgrd.50641, <http://dx.doi.org/10.1002/jgrd.50641>, 2013.
- Konwar, M., Mahes Kumar, R. S., Kulkarni, J. R., Freud, E., Goswami, B. N., and Rosenfeld, D.: Aerosol control on depth of warm rain in convective clouds, *Journal of Geophysical Research: Atmospheres*, 117, n/a–n/a, doi:10.1029/2012JD017585, <http://dx.doi.org/10.1029/2012JD017585>, d13204, 2012.
- 25 Luebke, A. E., Afchine, A., Costa, A., Grooß, J.-U., Meyer, J., Rolf, C., Spelten, N., Avallone, L. M., Baumgardner, D., and Krämer, M.: The origin of midlatitude ice clouds and the resulting influence on their microphysical properties, *Atmospheric Chemistry and Physics*, 16, 5793–5809, doi:10.5194/acp-16-5793-2016, <http://www.atmos-chem-phys.net/16/5793/2016/>, 2016.
- 30 Marshak, A., Platnick, S., Varnai, T., Wen, G. Y., and Cahalan, R. F.: Impact of three-dimensional radiative effects on satellite retrievals of cloud droplet sizes, *J. Geophys. Res.*, 111, 2006.
- Martins, J. V., Marshak, A., Remer, L. A., Rosenfeld, D., Kaufman, Y. J., Fernandez-Borda, R., Koren, I., Correia, A. L., Zubko, V., and Artaxo, P.: Remote sensing the vertical profile of cloud droplet effective radius, thermodynamic phase, and temperature, *Atmos. Chem. Phys.*, 11, 9485–9501, doi:10.5194/acp-11-9485-2011, 2011.
- 35 Meyer, J.: Ice Crystal Measurements with the New Particle Spectrometer NIXE-CAPS, Dr. (univ.), Jülich, <http://juser.fz-juelich.de/record/22871>, record converted from VDB: 12.11.2012; Wuppertal, Univ., Diss., 2012, 2012.
- Nicolet, M., Stetzer, O., and Lohmann, U.: Depolarization ratios of single ice particles assuming finite circular cylinders, *Appl. Opt.*, 46, 4465–4476, doi:10.1364/AO.46.004465, <http://ao.osa.org/abstract.cfm?URI=ao-46-20-4465>, 2007.
- Pavolonis, M. J.: Advances in Extracting Cloud Composition Information from Spaceborne Infrared Radiances – A Robust Alternative to Brightness Temperatures. Part I: Theory, *Journal of Applied Meteorology and Climatology*, 49, 1992–2012, doi:10.1175/2010JAMC2433.1, <http://dx.doi.org/10.1175/2010JAMC2433.1>, 2010.
- Pierluissi, J. and Peng, G.-S.: New molecular transmission band models for LOWTRAN, *Opt. Eng.*, 24, 541–547, 1985.
- 5 Pilewskie, P. and Twomey, S.: Discrimination of ice from water in clouds by optical remote sensing, *Atmos. Res.*, 21, 113–122, 1987.
- Platnick, S., King, M., Ackerman, S., Menzel, W., Baum, B., Riedi, J., and Frey, R.: The MODIS cloud products: Algorithms and examples from TERRA, *IEEE Trans. Geosci. Remote Sens.*, 41, 459–473, 2003.
- Platnick, S., Meyer, K. G., King, M. D., Wind, G., Amarasinghe, N., Marchant, B., Arnold, G. T., Zhang, Z., Hubanks, P. A., Holz, R. E., Yang, P., Ridgway, W. L., and Riedi, J.: The MODIS Cloud Optical and Microphysical Products: Collection 6 Updates and Examples
- 10 From Terra and Aqua, *IEEE Transactions on Geoscience and Remote Sensing*, 55, 502–525, doi:10.1109/TGRS.2016.2610522, 2017.
- Ricchiuzzi, P. and Gautier, C.: Investigation of the effect of surface heterogeneity and topography on the radiation environment of Palmer Station, Antarctica, with a hybrid 3-D radiative transfer model, *J. Geophys. Res.*, 103, 6161–6178, 1998.
- Rosenfeld, D. and Feingold, G.: Explanations of discrepancies among satellite observations of the aerosol indirect effects, *Geophys. Res. Lett.*, 30, doi:10.1029/2003GL017684, 2003.
- 15 Rosenfeld, D. and Lensky, I. M.: Satellite-based insights into precipitation formation processes in continental and maritime convective clouds, *Bull. Amer. Meteor. Soc.*, 79, 2457–2476, 1998.

- Rosenfeld, D. and Woodley, W. L.: Deep convective clouds with sustained supercooled liquid water down to -37.5 C, *Nature*, 405, 440–442, 2000.
- Rosenfeld, D. and Woodley, W. L.: Spaceborne Inferences of Cloud Microstructure and Precipitation Processes: Synthesis, Insights, and Implications, *Meteorological Monographs*, 51, 59–80, doi:10.1175/0065-9401(2003)029<0059:CSIOCM>2.0.CO;2, [http://dx.doi.org/10.1175/0065-9401\(2003\)029<0059:CSIOCM>2.0.CO;2](http://dx.doi.org/10.1175/0065-9401(2003)029<0059:CSIOCM>2.0.CO;2), 2003.
- Rosenfeld, D., Lohmann, U., Raga, G. B., O'Dowd, C. D., Kulmala, M., Fuzzi, S., Reissell, A., and Andreae, M. O.: Flood or drought: How do aerosols affect precipitation?, *Science*, 321, 1309–1313, 2008.
- Rosenfeld, D., Liu, G., Yu, X., Zhu, Y., Dai, J., Xu, X., and Yue, Z.: High-resolution (375 m) cloud microstructure as seen from the NPP/VIIRS satellite imager, *Atmos. Chem. Phys.*, 14, 2479–2496, doi:10.5194/acp-14-2479-2014, <http://www.atmos-chem-phys.net/14/2479/2014/>, 2014.
- Schnaiter, M., Järvinen, E., Vochezer, P., Abdelmonem, A., Wagner, R., Jourdan, O., Mioche, G., Shcherbakov, V. N., Schmitt, C. G., Tricoli, U., Ulanowski, Z., and Heymsfield, A. J.: Cloud chamber experiments on the origin of ice crystal complexity in cirrus clouds, *Atmospheric Chemistry and Physics*, 16, 5091–5110, doi:10.5194/acp-16-5091-2016, <http://www.atmos-chem-phys.net/16/5091/2016/>, 2016.
- Schwarzmaier, T., Baumgartner, A., Gege, P., Köhler, C., and Lenhard, K.: DLR's New Traceable Radiance Standard "RASTA", in: *International Geoscience and Remote sensing Symposium (IEEE, 2012)*, pp. 1–4, 2012.
- Seiz, G. and Davies, R.: Reconstruction of cloud geometry from multi-view satellite images, *REMOTE SENSING OF ENVIRONMENT*, 100, 143–149, doi:10.1016/j.rse.2005.09.016, 2006.
- Shettle, E.: Comments on the use of LOWTRAN in transmission calculations for sites with the ground elevated relative to sea level, *Appl. Opt.*, 28, 1451–1452, 1989.
- Tao, W.-K., Starr, D., Hou, A., Newman, P., and Sud, Y.: A cumulus parameterization workshop, *Bull. Amer. Meteorol. Soc.*, 84, 1055–1062, 2003.
- Tao, W.-K., Chen, J.-P., Li, Z., Wang, C., and Zhang, C.: Impact of aerosols on convective clouds and precipitation, *Reviews of Geophysics*, 50, 1–62, doi:10.1029/2011RG000369, <http://dx.doi.org/10.1029/2011RG000369>, rG2001, 2012.
- Twomey, S.: The influence of pollution on the shortwave albedo of clouds, *J. Atmos. Sci.*, 34, 1149–1152, 1977.
- Voigt, C., Schumann, U., Minikin, A., Abdelmonem, A., Afchine, A., Borrmann, S., Boettcher, M., Buchholz, B., Bugliaro, L., Costa, A., Curtius, J., Dollner, M., Dörnbrack, A., Dreiling, V., Ebert, V., Ehrlich, A., Fix, A., Forster, L., Frank, F., Fütterer, D., Giez, A., Graf, K., Groß, J.-U., Groß, S., Heimerl, K., Heinold, B., Hüneke, T., Järvinen, E., Jurkat, T., Kaufmann, S., Kenntner, M., Klingebiel, M., Klimach, T., Kohl, R., Krämer, M., Krisna, T. C., Luebke, A., Mayer, B., Mertes, S., Molleker, S., Petzold, A., Pfeilsticker, K., Port, M., Rapp, M., Reutter, P., Rolf, C., Rose, D., Sauer, D., Schäfler, A., Schlage, R., Schnaiter, M., Schneider, J., Spelten, N., Spichtinger, P., Stock, P., Walser, A., Weigel, R., Weinzierl, B., Wendisch, M., Werner, F., Wernli, H., Wirth, M., Zahn, A., Ziereis, H., and Zöger, M.: ML-CIRRUS - The airborne experiment on natural cirrus and contrail cirrus with the high-altitude long-range research aircraft HALO, *Bulletin of the American Meteorological Society*, doi:10.1175/BAMS-D-15-00213.1, <http://dx.doi.org/10.1175/BAMS-D-15-00213.1>, 2017.
- Wendisch, M., Pöschl, U., Andreae, M. O., Machado, L. A. T., Albrecht, R., Schlager, H., Rosenfeld, D., Martin, S. T., Abdelmonem, A., Afchine, A., Araujo, A., Artaxo, R., Aufmhoff, H., Barbosa, H. M. J., Borrmann, S., Braga, R., Buchholz, B., Cecchini, M. A., Costa, A., Curtius, J., Dollner, M., Dorf, M., Dreiling, V., Ebert, V., Ehrlich, A., Ewald, F., Fisch, G., Fix, A., Frank, F., Fütterer, D., Heckl, C., Heidelberg, F., Hüneke, T., Jäkel, E., Järvinen, E., Jurkat, T., Kanter, S., Kästner, U., Kenntner, M., Kesselmeier, J., Klimach, T., Knecht, M., Kohl, R., Kölling, T., Krämer, M., Krüger, M., Krisna, T. C., Lavric, J. V., Longo, K., Mahnke, C., Manzi, A. O., Mayer, B., Mertes, S., Minikin, A., Molleker, S., Münch, S., Nillius, B., Pfeilsticker, K., Pöhlker, C., Roiger, A. E., Rose, D., Rosenow, D., Sauer,

- D., Schnaiter, M., Schneider, J., Schulz, C., de Souza, R. A. F., Spanu, A., Stock, P., Vila, D., Voigt, C., Walser, A., Walter, D., Weigel, R., Weinzierl, B., Werner, R., Yamasoe, M. A., Ziereis, H., Zinner, T., and Zöger, M.: The ACRIDICON-CHUVA campaign: Studying tropical deep convective clouds and precipitation over Amazonia using the new German research aircraft HALO, *Bull. Am. Meteorol. Soc.*, doi:10.1175/BAMS-D-14-00255.1, 2016.
- 770 Yuan, T., Martins, J. V., Li, Z., and Remer, L. A.: Estimating glaciation temperature of deep convective clouds with remote sensing data, *Geophys. Res. Lett.*, 37, doi:10.1029/2010GL042753, 2010.
- Zinner, T., Mannstein, H., and Tafferner, A.: Cb-TRAM: Tracking and monitoring severe convection from onset over rapid development to mature phase using multi-channel Meteosat-8 SEVIRI data, *Meteorology and Applied Physics*, submitted, 2006.
- 775 Zinner, T., Marshak, A., Lang, S., Martins, J. V., and Mayer, B.: Remote sensing of cloud sides of deep convection: towards a three-dimensional retrieval of cloud particle size profiles, *Atmos. Chem. Phys.*, 8, 4741–4757, 2008.

**Table 1.** Summary of presented flights with cloud side observations during the ACRIDICON–CHUVA campaign. The ranges of flight altitude and time refer to the studied cloud cases.

<u>Flight number</u>	<u>AC10</u>	<u>AC13</u>	<u>AC18</u>
<u>Aerosol conditions</u>	<u>moderate</u>	<u>polluted</u>	<u>moderate</u>
<u>AOD (MODIS)</u>	<u>0.4 - 0.5</u>	<u>0.5 - 0.6</u>	<u>0.3 - 0.4</u>
<u>Number of cloud cases</u>	<u>9</u>	<u>16</u>	<u>10</u>
<u>Flight altitude range (km)</u>	<u>7.4 - 10.4</u>	<u>5.2 - 9.3</u>	<u>1.4 - 14.0</u>
<u>Time range (UTC)</u>	<u>17:25 - 19:20</u>	<u>17:55 - 19:00</u>	<u>15:30 - 20:30</u>

**Table 2.** Cloud flag description of the NIXE-CAPS asphericity product after Costa et al. (2017). Group I: total concentration of particles 3-50  $\mu\text{m}$  is larger than  $3 \text{ cm}^{-3}$ , Group II: total concentration of particles 3-50  $\mu\text{m}$  is smaller than  $1 \text{ cm}^{-3}$  and total concentration of particles with size larger than 50  $\mu\text{m}$  is larger than  $0 \text{ cm}^{-3}$ .

Cloud flag	Temperature range ( $^{\circ}\text{C}$ )	Description
1.0	$> 0$	no aspherical particles detected; liquid
1.1	$> 0$	aspherical particles detected - could be ice or ash particles
2.0	$0 > T > -38$	no aspherical particles detected; liquid
2.1	$0 > T > -38$	aspherical particles detected, group I; mixed phase
2.2	$0 > T > -38$	aspherical particles detected, group II; ice
3.0	$< -38$	below homogeneous freezing threshold: all ice, no asphericity criterion; ice

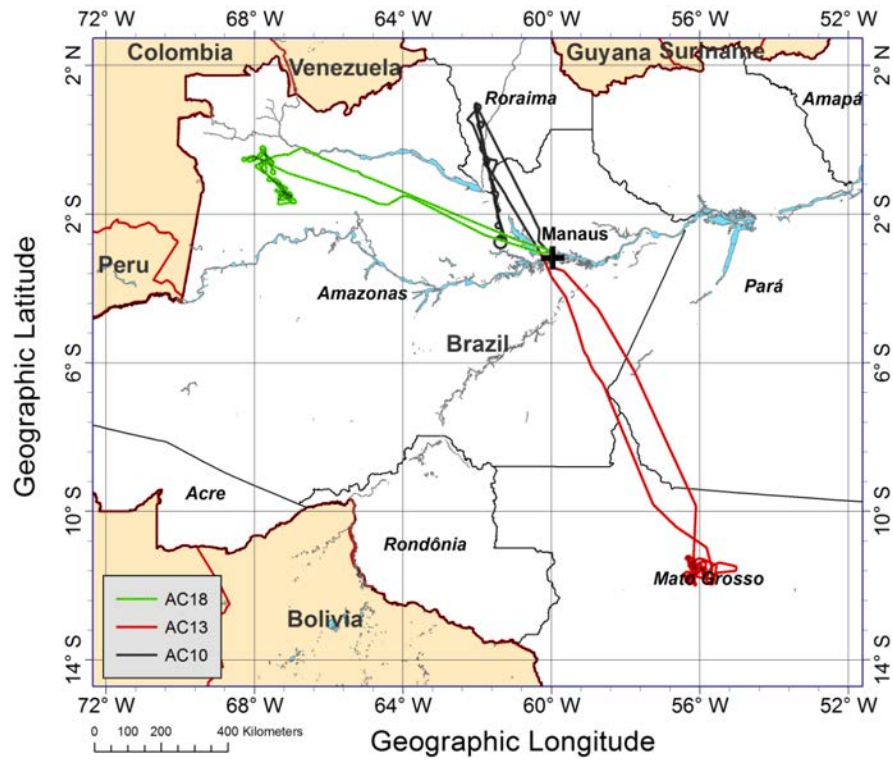


**Figure 1.** Flight tracks of AC10 (black), AC13 (red), and AC18 (green). The city of Manaus is indicated by the black cross.

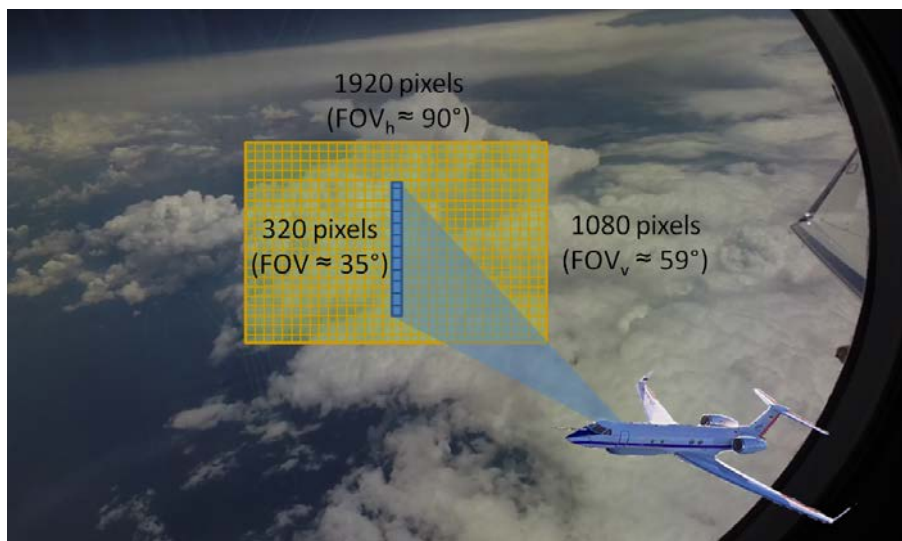


**Figure 2.** Schematics of cloud side observations by the imaging spectrometer specMACS (SWIR camera) and the GoPro camera. The individual field of views (FOVs) and corresponding number of spatial pixels are illustrated.

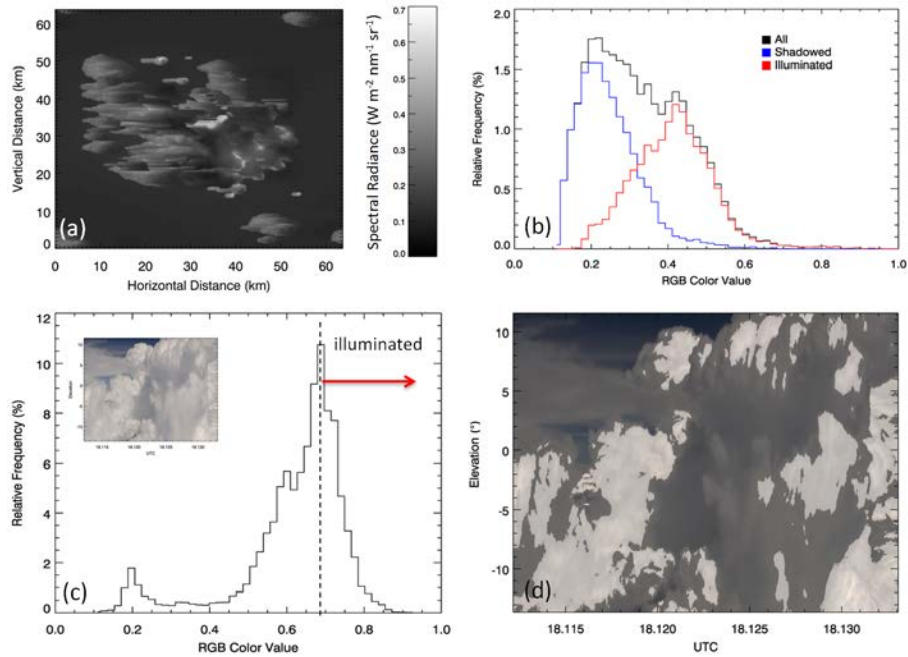


**Figure 3.** (a) Field of RGB color values from simulated spectral radiances for cloud side viewing geometry with a sensor elevation angle of  $10^\circ$  and a relative azimuth angle of  $60^\circ$ . (b) Histograms of RGB color values of the field shown in (a). (c) Histogram of RGB color values for a measured cloud scene shown in the [insert inset](#). (d) Identified illuminated cloud sides of the observed cloud scene are highlighted in brighter colors.

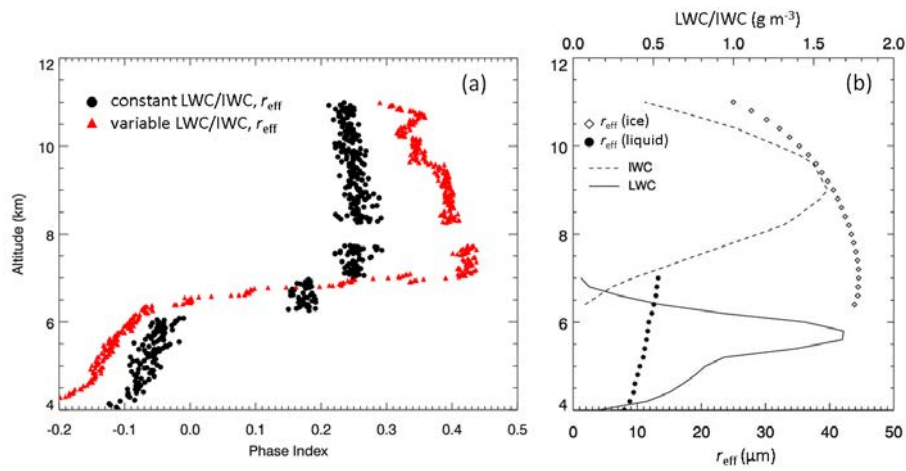


**Figure 4.** (a) Phase index derived for simulated clouds with variable LWC/IWC and effective radius and fixed values of microphysical properties. (b) Profile of corresponding cloud with variable LWC/IWC and  $r_{\text{eff}}$ .

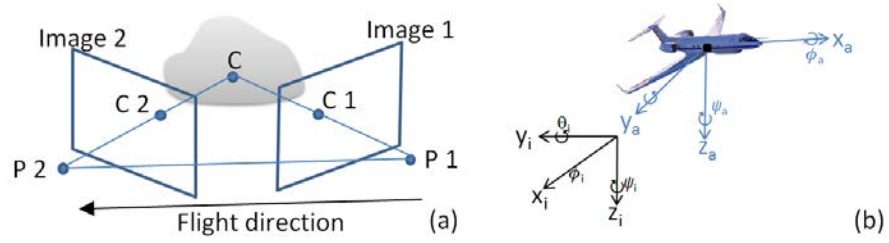


**Figure 5.** (a) Schematics of stereo-photogrammetric observations of cloud point C from aircraft position P1 and P2 with projected image points C1 and C2. (b) Illustration of aircraft and camera coordinate systems.

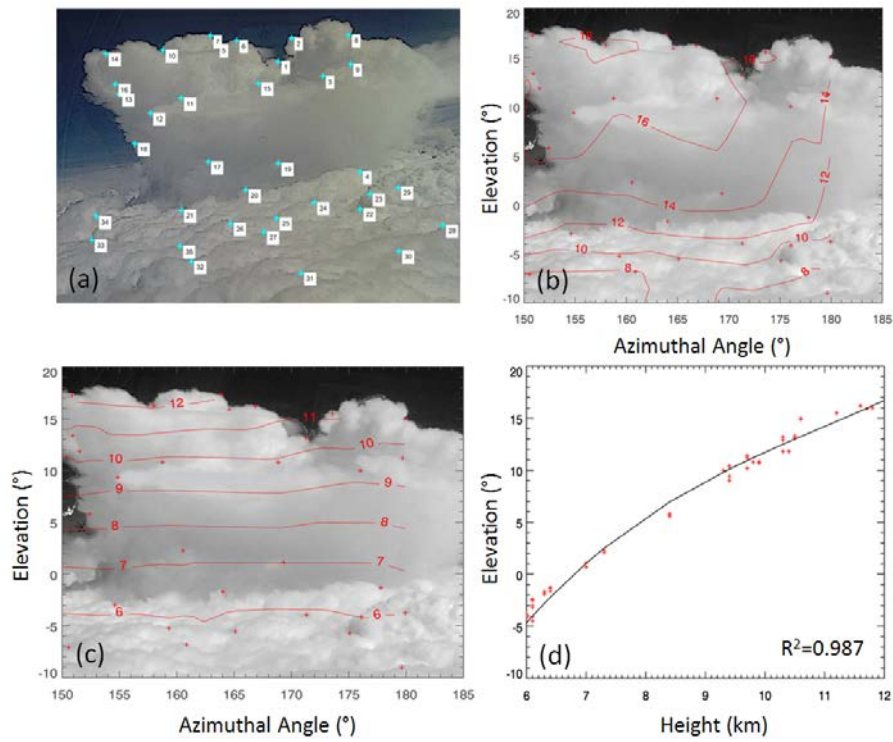


**Figure 6.** (a) Cloud image from GoPro camera with enhanced edges and selected tie points from 19 September 2014. (b) Calculated distances in km to the individual cloud points for the cloud scene displayed as isolines. (c) Corresponding isolines of calculated heights. (d) Relationship of height and elevation angle derived for the cloud case including a polynomial fit with a correlation coefficient of  $R^2 = 0.987$ .

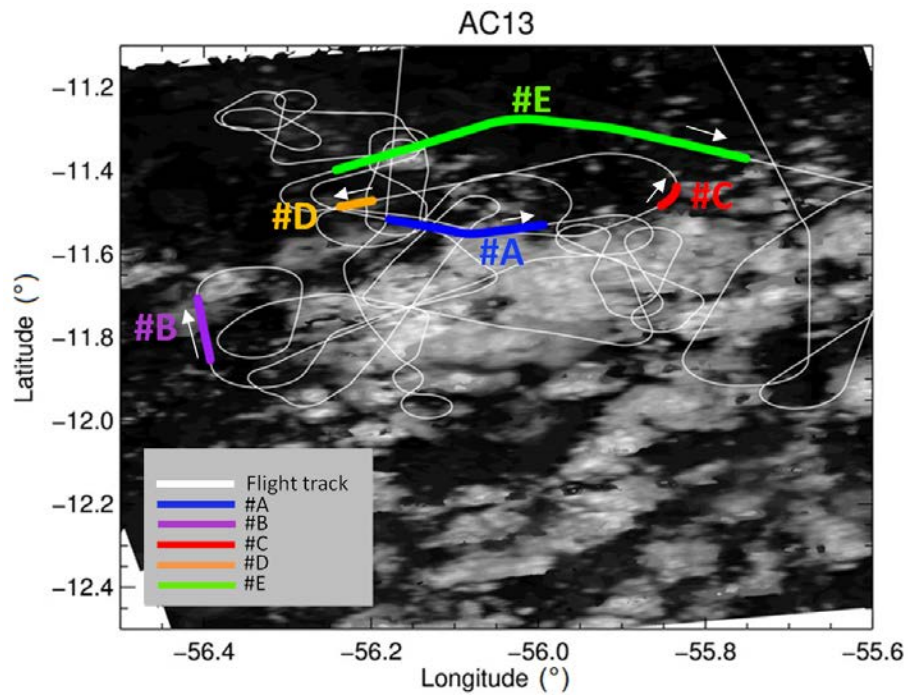


**Figure 7.** Flight track (white line) and selected time periods of cloud side observations during AC13 (19 September 2014). Additionally, the 250 m resolution product for channel 1 (620 - 670 nm) of the Aqua-MODIS instrument from 17:50 UTC is shown in the background. [Figure is similar as presented in Jäkel et al. \(2016\).](#)

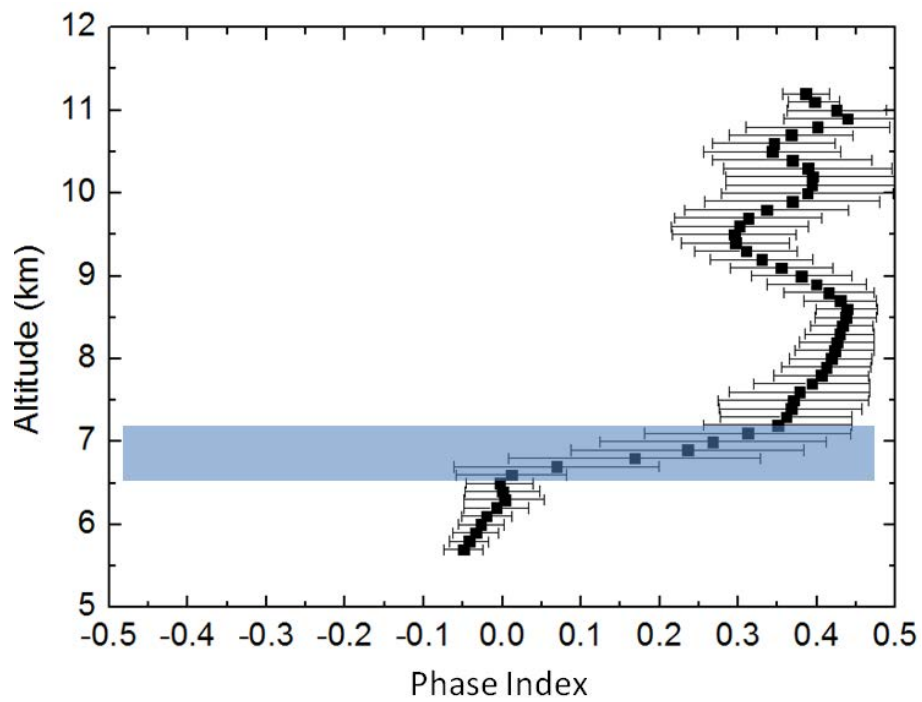


**Figure 8.** Mean phase index profile for cloud scene shown in Fig. 6. The mixed phase layer is indicated by the colored area.

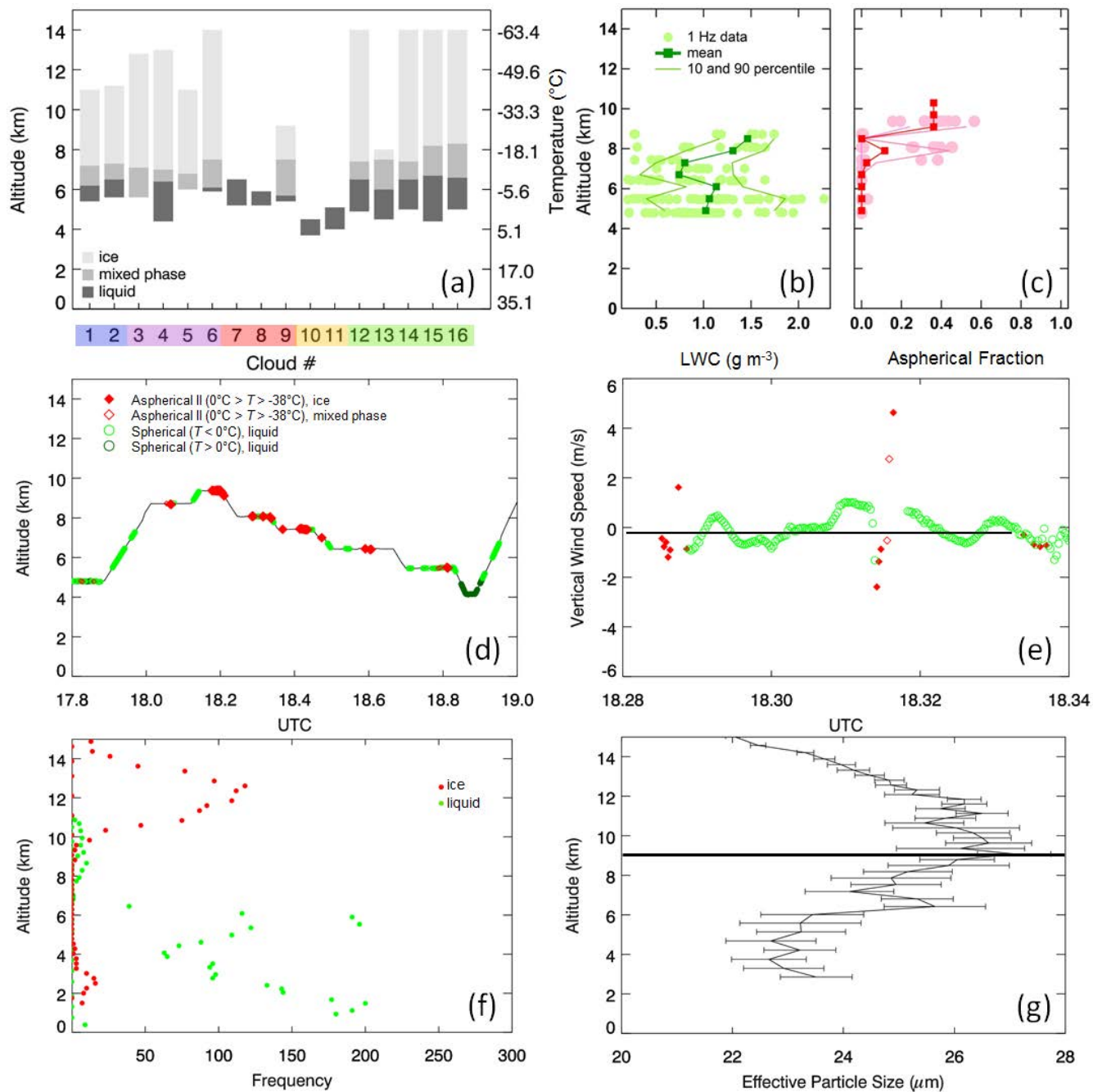


**Figure 9.** (a) Phase classification of studied clouds based on specMACS observations during flight AC13. (b) Profile of LWC measured with the hotwire probe between 17:50 and 19:00 UTC. (c) Aspherical fraction derived from CAS-DPOL in situ data. (d) NIXE-CAPS in situ measurements of liquid, mixed phase and ice, see Table 2 for definitions. Note, that time is given in decimal hours. (e) Short horizontal flight section in the upper part of the mixed phase layer showing the relation of vertical wind speed and classified asphericity of cloud particles. Symbols as in (d). (f) Classification of cloud phase (ice or liquid) from MODIS observations of cloud tops. (g) Mean profile of effective particle radius from ensemble method based on MODIS retrieval data of cloud top effective radius. The black horizontal line indicates the level of largest ice particles.

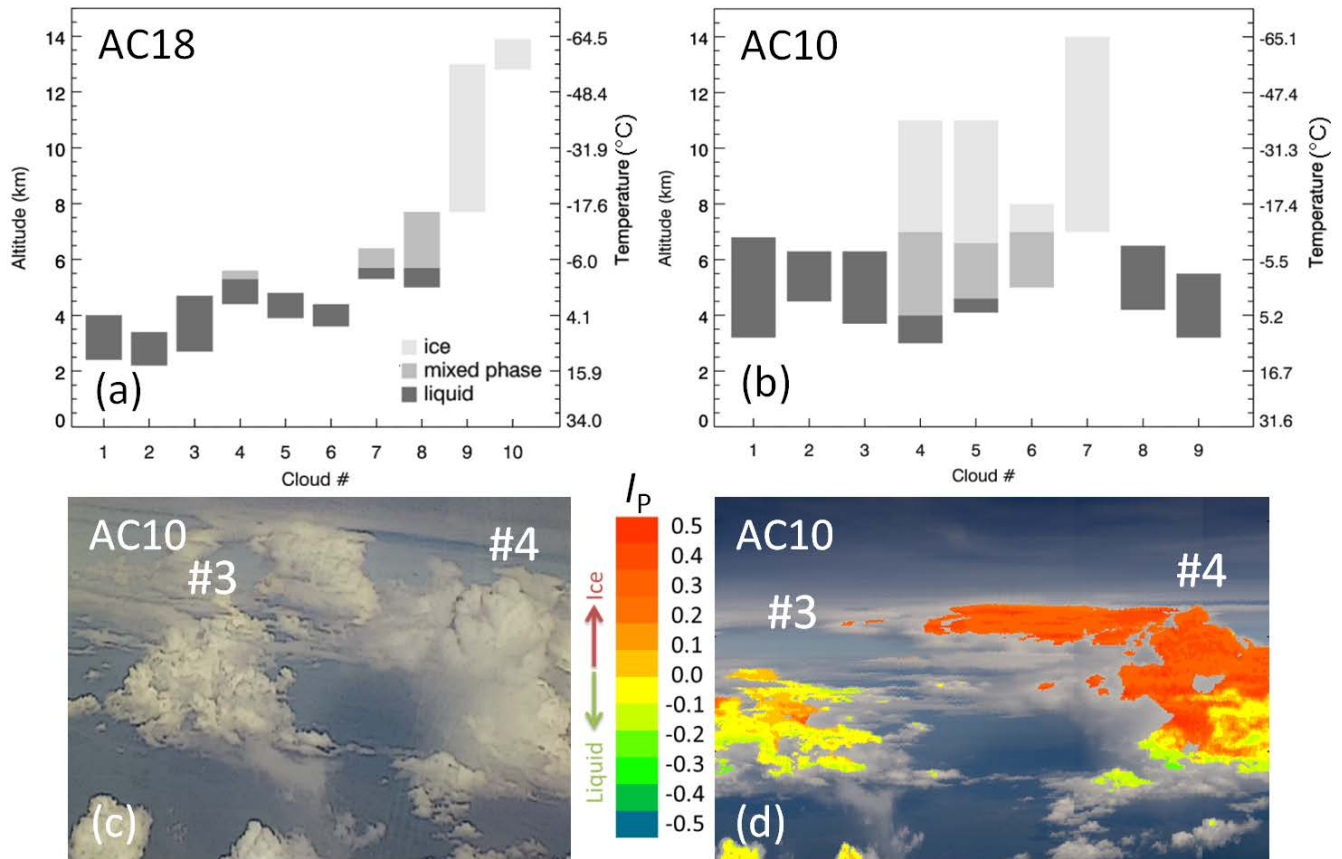


**Figure 10.** (a) Phase classification of studied clouds based on specMACS observations during flight AC18. (b) Same as (a) but for AC10. (c) GoPro image of cloud scene during AC10. (d) Phase index as derived from specMACS during AC10 for illustrated clouds from (c).